

Exact Thermal Properties of Integrable Spin Chains

Michał Białończyk¹, Fernando J. Gómez-Ruiz^{2,3}, Adolfo del Campo^{4,2,5,6,*}

1 Institute of Physics, Jagiellonian University, Łojasiewicza 11, 30-348 Kraków, Poland

2 Donostia International Physics Center, E-20018 San Sebastián, Spain

3 Departamento de Física, Universidad de Los Andes, A.A. 4976, Bogotá, Colombia

4 Department of Physics and Materials Science, University of Luxembourg, L-1511 Luxembourg, G. D. Luxembourg

5 IKERBASQUE, Basque Foundation for Science, E-48013 Bilbao, Spain

6 Department of Physics, University of Massachusetts, Boston, MA 02125, USA

* adolfo.delcampo@uni.lu

May 21, 2021

Abstract

An exact description of integrable spin chains at finite temperature is provided using an elementary algebraic approach in the complete Hilbert space of the system. We focus on spin chain models that admit a description in terms of free fermions, including paradigmatic examples such as the one-dimensional transverse-field quantum Ising and XY models. The exact partition function is derived and compared with the ubiquitous approximation in which only the positive parity sector of the energy spectrum is considered. Errors stemming from this approximation are identified in the neighborhood of the critical point at low temperatures. We further provide the full counting statistics of a wide class of observables at thermal equilibrium and characterize in detail the thermal distribution of the kink number and transverse magnetization in the transverse-field quantum Ising chain.

Contents

1	Introduction	2
2	Full Diagonalization of Spin-$\frac{1}{2}$ XY Model	3
2.1	Mathematical tools for the complete Hilbert space	6
3	The Canonical Partition Function	9
4	Full Counting Statistics in Integrable Spin Chains	13
4.1	Probability distribution of the number of kinks at thermal equilibrium	16
4.2	Probability distribution for the transverse magnetization at thermal equilibrium	21
5	Conclusion	27
A	Proof Proposition 2: Identities for Traces	28
	References	28

1 Introduction

Quantum many-body spin systems that are exactly solvable and exhibit a quantum phase transition have been key to advance our understanding of critical phenomena in the quantum domain. Among them, the one-dimensional XY model and the closely-related transverse-field quantum Ising model (TFQIM) occupy a unique status, and are paradigmatic test-beds of quantum critical behavior [1–4]. They belong to a family of models that admit an exact diagonalization by a combination of Jordan-Wigner and Fourier transformations, yielding a formulation of the system in terms of free fermions [5, 6]. These family of quasi-free fermion models include as well the Kitaev spin model in one dimension and on a honeycomb lattice [7], among other examples [1, 2, 4].

Quasi-free fermion models have indeed been instrumental in exploring both equilibrium and nonequilibrium properties. At equilibrium, the study of the ground-state critical behavior was shown to be of relevance to the characterization of the system at finite temperature [8–10]. Out of equilibrium, these models have been used to explore the dynamics following a sudden quench (e.g., of the magnetic field). The study of finite-time quenches was key to establish the validity of the universal Kibble-Zurek mechanism in the quantum domain, and confirm the power-law scaling of the number of kinks by driving the ground-state of a paramagnet across the phase transition [11, 12], as reported in a variety of experiments [13–16]. These results have also been extended to nonlinear quenches [17, 18] and inhomogeneous systems [19–23], while their breakdown has been characterized in open systems [24–26]. More recently, it has been shown that signatures of universality are present in the full kink-number distribution and that all cumulants scale as a universal power-law of the quench time [16, 27–31]. The universal dynamics of defect formation is not always desirable, and a variety of works have been devoted to circumvent it using diverse control protocols [32–42], beyond the use of nonlinear quenches and inhomogeneous driving. In addition, quasi-free fermion models have been discussed in the context of quantum thermodynamics, as a test-bed to explore work statistics and fluctuation theorems [43–46] and as a working substance in a quantum thermodynamic cycle [47].

Quasi-free fermion models provided an effective description of a variety of condensed-matter systems, where they can be realized with high accuracy in [48]. They are further amenable to quantum simulation with trapped ions [49–53], ultracold gases in optical lattices [54] and superconducting qubits [55]. Digital quantum simulation provides yet another avenue for their study in the laboratory [15, 56–58].

In many applications, it is generally desirable to consider a thermal state and analyze the finite-temperature behavior. For a given observable, full information about the eigenvalue distribution and its cumulants can be extracted from the characteristic function. An ubiquitous approximation in such description exploits the parity symmetry of the TFQIM and XY modes, focusing on the positive-parity subspace, while disregarding the rest of the spectrum [1–4, 44, 59–62]. We refer to it as the positive-parity approximation or PPA for short. The PPA is considered to be accurate in the thermodynamic limit [63], invoked in many works [6, 64]. However, *even in the thermodynamic limit*, an exact treatment requires taking into account parity properly and at finite temperature both subspaces are populated. Katsura derived the exact partition function for a finite-size spin chain in 1962 [63]. Kapitonov and Il’inskii provided an alternative derivation of the closed form expression of the exact partition function using functional integrals over Grassmann variables [65]. More recently, Fei and Quan [45] used group theory methods to calculate the exact partition function and quantum work distribution.

In this manuscript, we first elaborate on these results providing an elementary derivation of the

75 exact partition function based on the structure of the Hilbert space. Using this approach, we next
 76 provide exact expressions for the eigenvalue distribution (full counting statistics) of a wide class of
 77 observables at thermal equilibrium. We present step-by-step worked examples deriving the exact
 78 moment generating function for important observables: the kink number and transverse magne-
 79 tization. In addition, we analyze finite-size effects and illustrate discrepancies between results
 80 obtained using the PPA for the partition function and the exact partition function for small systems
 81 spins. These discrepancies are of direct relevance to typical system sizes in current experimen-
 82 tal realizations of spin systems [66, 67]. For convenience of the reader interested in using the
 83 final results of a calculation, the corresponding explicit formulas are summarized in boxes that are
 84 self-contained and make little or no reference to the rest of the manuscript.

85 2 Full Diagonalization of Spin- $\frac{1}{2}$ XY Model

86 We consider the anisotropic one-dimensional XY Hamiltonian for spins $1/2$ in a transverse mag-
 87 netic field g . The Hamiltonian reads:

$$\hat{\mathcal{H}}(g, \gamma) = -J \left[\sum_{n=1}^L \left(\frac{1+\gamma}{2} \right) \hat{X}_n \hat{X}_{n+1} + \left(\frac{1-\gamma}{2} \right) \hat{Y}_n \hat{Y}_{n+1} + g \hat{Z}_n \right]. \quad (1)$$

88 Here, J parameterizes the ferromagnetic ($J > 0$) or antiferromagnetic ($J < 0$) exchange interaction
 89 between nearest neighbors; we set the energy scale by taking $J = 1$. The dimensionless anisotropic
 90 parameter in the XY plane is given by $\gamma > 0$ and L is the number of sites in the chain. For $\gamma = 1$, the
 91 Hamiltonian (1) corresponds to the Ising model in a transverse magnetic field, which possesses
 92 a \mathbb{Z}_2 symmetry. The limit $\gamma = 0$ describes the isotropic XY model. For the anisotropic case
 93 $0 < \gamma \leq 1$ the model belongs to the Ising universality class, and its phase diagram is determined
 94 by the ratio $\nu = g/J$. When $\nu > 1$, the magnetic field dominates over the nearest-neighbor
 95 coupling, polarizing the spins along the z direction. This corresponds to a paramagnetic state, with
 96 zero magnetization in the xy plane. By contrast, in the regime $0 \leq \nu < 1$ the ground state of the
 97 system corresponds to a ferromagnetic configuration with polarization along the xy plane. These
 98 phases are separated by a quantum phase transition (QPT) at the critical point $\nu = 1$. Finally, for
 99 the isotropic case $\gamma = 0$, a QPT is observed between gapless ($\nu < 1$) and ferromagnetic ($\nu > 1$)
 100 phases.

101 The operators \hat{X}_n , \hat{Y}_n , and \hat{Z}_n are matrices of order 2^L defined by the relations

$$\begin{aligned} \hat{X}_n &= \hat{\mathbb{1}}_1 \otimes \dots \otimes \hat{\mathbb{1}}_{n-1} \otimes \hat{\sigma}_n^x \otimes \hat{\mathbb{1}}_{n+1} \otimes \dots \otimes \hat{\mathbb{1}}_L, \\ \hat{Y}_n &= \hat{\mathbb{1}}_1 \otimes \dots \otimes \hat{\mathbb{1}}_{n-1} \otimes \hat{\sigma}_n^y \otimes \hat{\mathbb{1}}_{n+1} \otimes \dots \otimes \hat{\mathbb{1}}_L, \\ \hat{Z}_n &= \hat{\mathbb{1}}_1 \otimes \dots \otimes \hat{\mathbb{1}}_{n-1} \otimes \hat{\sigma}_n^z \otimes \hat{\mathbb{1}}_{n+1} \otimes \dots \otimes \hat{\mathbb{1}}_L. \end{aligned} \quad (2)$$

102 Here, $\hat{\sigma}_n^\alpha$ denotes the Pauli operator at site n along the axis $\alpha = x, y, z$, $\hat{\mathbb{1}}_n$ is the identity matrix of
 103 order 2 at the site n , and periodic boundary conditions are assumed, $\hat{\sigma}_{L+1}^\alpha = \hat{\sigma}_1^\alpha$. A standard way
 104 to diagonalize the Hamiltonian in Eq. (1) relies on introducing a new set of Fermionic operators
 105 given by

$$\begin{aligned} \hat{\sigma}_n^x &= (\hat{c}_n^\dagger + \hat{c}_n) \prod_{m < n} (\hat{\mathbb{1}}_m - 2\hat{c}_m^\dagger \hat{c}_m), \\ \hat{\sigma}_n^y &= -i(\hat{c}_n^\dagger - \hat{c}_n) \prod_{m < n} (\hat{\mathbb{1}}_m - 2\hat{c}_m^\dagger \hat{c}_m), \\ \hat{\sigma}_n^z &= \hat{\mathbb{1}}_n - 2\hat{c}_n^\dagger \hat{c}_n. \end{aligned} \quad (3)$$

106 These expressions represent the well-known Jordan-Wigner transformation [68]. Here, \hat{c}_n and \hat{c}_n^\dagger
 107 are ladder Fermionic operators at site n , which satisfy anti-commutation relations $\{\hat{c}_i, \hat{c}_j^\dagger\} = \delta_{ij}$

108 and $\{\hat{c}_i, \hat{c}_j\} = \{\hat{c}_i^\dagger, \hat{c}_j^\dagger\} = 0$. This is in contrast to the Pauli matrices, which satisfy commutation
 109 relations $[\hat{\sigma}_n^\dagger, \hat{\sigma}_m^-] = \delta_{n,m} \hat{\sigma}_n^z$ and $[\hat{\sigma}_n^z, \hat{\sigma}_m^\pm] = \pm 2\delta_{n,m} \hat{\sigma}_n^\pm$ with $\hat{\sigma}_n^\pm = \hat{\sigma}_n^x \pm i\hat{\sigma}_n^y$. With periodic boundary
 110 conditions in the spin representation, the Fermionic operators \hat{c}_n and \hat{c}_n^\dagger satisfy nontrivial boundary
 111 conditions

$$\hat{c}_{L+1}^\dagger = (-1)^{\hat{N}} \hat{c}_1^\dagger, \quad \hat{c}_{L+1} = (-1)^{\hat{N}} \hat{c}_1, \quad (4)$$

112 where $\hat{N} = \sum_{n=1}^L \hat{c}_n^\dagger \hat{c}_n$ is the Fermionic number operator. By direct substitution of Eq. (3) into
 113 Eq. (1), the Hamiltonian can be written as a quadratic form

$$\begin{aligned} \hat{H}(g, \gamma) = & - \sum_{n=1}^{L-1} \left[\hat{c}_n^\dagger \hat{c}_{n+1} + \hat{c}_{n+1}^\dagger \hat{c}_n + \gamma (\hat{c}_n^\dagger \hat{c}_{n+1}^\dagger + \hat{c}_{n+1} \hat{c}_n) \right] \\ & + \hat{\Pi} \left[\hat{c}_L^\dagger \hat{c}_1 + \hat{c}_1^\dagger \hat{c}_L + \gamma (\hat{c}_L^\dagger \hat{c}_1^\dagger + \hat{c}_1 \hat{c}_L) \right] - g \sum_{n=1}^L (\hat{\mathbb{1}}_n - 2\hat{c}_n^\dagger \hat{c}_n). \end{aligned} \quad (5)$$

114 Here, the parity operator $\hat{\Pi}$ is given by $(-1)^{\hat{N}} = \exp(i\pi\hat{N})$ and has eigenvalues ± 1 . The parity op-
 115 erator anticommutes with the creation \hat{c}_n^\dagger and annihilation \hat{c}_n Fermionic operators, $\{(-1)^{\hat{N}}, \hat{c}_n^\dagger\} =$
 116 $\{(-1)^{\hat{N}}, \hat{c}_n\} = 0$, and therefore, it commutes with any operator bilinear in \hat{c}_n^\dagger and \hat{c}_n . The Hamil-
 117 tonian given by Eq. (5) does not conserve the number of Fermionic excitations. However, it is
 118 well-known that the TFQIM has a global \mathbb{Z}_2 symmetry and, thus, the parity operator $\hat{\Pi}$ commutes
 119 with the Hamiltonian. As a result, the total Hilbert space is split into the direct sum of two 2^{L-1}
 120 dimensional subspaces of positive (+1) and negative (-1) parity. Using the projectors $\hat{\Pi}^\pm$,

$$\hat{\Pi}^\pm = \frac{1}{2} \left[\hat{\mathbb{1}} \pm (-1)^{\hat{N}} \right], \quad (6)$$

121 the Hamiltonian in Eq. (5) is represented in the form

$$\hat{H} = \hat{H}^+ \hat{\Pi}^+ + \hat{H}^- \hat{\Pi}^-, \quad (7)$$

122 with the reduced Hamiltonians \hat{H}^\pm being given by

$$\hat{H}^\pm(g, \gamma) = - \sum_{n=1}^L \left[\hat{c}_n^\dagger \hat{c}_{n+1} + \hat{c}_{n+1}^\dagger \hat{c}_n + \gamma (\hat{c}_n^\dagger \hat{c}_{n+1}^\dagger + \hat{c}_{n+1} \hat{c}_n) + g (\hat{\mathbb{1}}_n - 2\hat{c}_n^\dagger \hat{c}_n) \right]. \quad (8)$$

123 A subtle difference between \hat{H}^+ and \hat{H}^- is found in the boundary conditions for the Fermion
 124 operators. \hat{H}^+ obeys antiperiodic boundary conditions ($\hat{c}_{L+1} = -\hat{c}_1$ and $\hat{c}_{L+1}^\dagger = -\hat{c}_1^\dagger$) while \hat{H}^-
 125 satisfies periodic boundary conditions ($\hat{c}_{L+1} = \hat{c}_1$ and $\hat{c}_{L+1}^\dagger = \hat{c}_1^\dagger$). The Hamiltonian given by
 126 Eq. (8) is quadratic in the Fermionic operators and is thus exactly diagonalizable using Fourier and
 127 Bogoliubov transformations [64, 69–71]. We expand the operator \hat{c}_n via a Fourier transformation
 128 in momentum space,

$$\hat{c}_n = \frac{e^{-in\pi/4}}{\sqrt{L}} \sum_{k \in \mathbf{K}^\pm} \hat{c}_k \exp(ink), \quad \hat{c}_n^\dagger = \frac{e^{in\pi/4}}{\sqrt{L}} \sum_{k \in \mathbf{K}^\pm} \hat{c}_k^\dagger \exp(-ink). \quad (9)$$

129 The wavevector k takes values in the positive (\mathbf{K}^+) and negative (\mathbf{K}^-) parity sectors

$$\mathbf{K}^+ = \left\{ k \left| \frac{\pi}{L} (2m-1), \quad m = -\frac{L}{2} + 1, -\frac{L}{2} + 2, \dots, \frac{L}{2} - 1, \frac{L}{2} \right. \right\}, \quad (10)$$

$$\mathbf{K}^- = \left\{ k \left| \frac{2\pi}{L} m, \quad m = -\frac{L}{2} + 1, -\frac{L}{2} + 2, \dots, \frac{L}{2} - 1, \frac{L}{2} \right. \right\}. \quad (11)$$

130 We emphasize that Eqs. (10) and (11) are valid for an even and odd number of particles in the
 131 chain. In the following analysis, we consider even L . In this way, the modes $\mathbf{k} = 0$ and $\mathbf{k} = \pi$
 132 are included in the negative parity sector. For even L , we can rewrite conveniently the momentum
 133 values as

$$\mathbf{K}^+ = \left\{ \pm \frac{\pi}{L}, \pm \frac{3\pi}{L}, \pm \frac{5\pi}{L}, \dots, \pm \frac{\pi(L-1)}{L} \right\} = \mathbf{k}^+ \cup \{-\mathbf{k}^+\},$$

$$\mathbf{K}^- = \left\{ 0, \pm \frac{2\pi}{L}, \pm \frac{4\pi}{L}, \dots, \pm \frac{\pi(L-2)}{L}, \pi \right\} = \mathbf{k}^- \cup \{-\mathbf{k}^-\} \cup \{0, \pi\},$$

134 with

$$\mathbf{k}^+ = \left\{ \frac{\pi}{L}, \frac{3\pi}{L}, \dots, \frac{\pi(L-1)}{L} \right\}, \quad \text{and} \quad \mathbf{k}^- = \left\{ \frac{2\pi}{L}, \frac{4\pi}{L}, \dots, \frac{\pi(L-2)}{L} \right\}. \quad (12)$$

135 By direct substitution of Eq. (9) into Eq. (8), the reduced Hamiltonians \hat{H}^+ and \hat{H}^- are expressed
 136 in terms of \hat{c}_k and \hat{c}_k^\dagger as

$$\hat{H}^+(g, \gamma) = \sum_{k \in \mathbf{k}^+} \hat{H}_k(g, \gamma),$$

$$\hat{H}^-(g, \gamma) = \sum_{k \in \mathbf{k}^-} \hat{H}_k(g, \gamma) + \hat{H}_0(g) + \hat{H}_\pi(g), \quad (13)$$

137 where

$$\hat{H}_k(g, \gamma) = 2 \left[(g - \cos(k)) (\hat{c}_k^\dagger \hat{c}_k - \hat{c}_{-k} \hat{c}_{-k}^\dagger) + \gamma \sin(k) (\hat{c}_k^\dagger \hat{c}_{-k}^\dagger - \hat{c}_{-k} \hat{c}_k) \right],$$

$$\hat{H}_0(g) = (g - 1) (\hat{c}_0^\dagger \hat{c}_0 - \hat{c}_0 \hat{c}_0^\dagger), \quad (14)$$

$$\hat{H}_\pi(g) = (g + 1) (\hat{c}_\pi^\dagger \hat{c}_\pi - \hat{c}_\pi \hat{c}_\pi^\dagger).$$

138 We next make use of a Bogoliubov transformation, and define a new set of fermion operators $\hat{\gamma}_k$
 139 and $\hat{\gamma}_k^\dagger$ given by

$$\hat{\gamma}_k = u_k \hat{c}_k - i v_k \hat{c}_{-k}^\dagger, \quad \hat{\gamma}_k^\dagger = u_k \hat{c}_k^\dagger + i v_k \hat{c}_{-k}, \quad (15)$$

140 where the real numbers u_k and v_k satisfy $u_k = u_{-k}$, $v_k = -v_{-k}$ and $|u_k|^2 + |v_k|^2 = 1$. The canonical
 141 anti-commutation relations for the operators \hat{c}_k and \hat{c}_k^\dagger imply that the same relations are also sat-
 142 isfied by $\hat{\gamma}_k$ and $\hat{\gamma}_k^\dagger$, that is, $\{\hat{\gamma}_k, \hat{\gamma}_{k'}^\dagger\} = \delta_{k,k'}$, and $\{\hat{\gamma}_k^\dagger, \hat{\gamma}_{k'}^\dagger\} = \{\hat{\gamma}_k, \hat{\gamma}_{k'}\} = 0$. By direct substitution of
 143 the Bogoliubov transformations into Eq. (13), after a some algebra, we obtain

$$\hat{H}_k(g, \gamma) = 2 \hat{\gamma}_k^\dagger \hat{\gamma}_k \left[u_k^2 (\cos(k) - g) + \gamma \sin(k) u_k v_k \right]$$

$$+ 2 \hat{\gamma}_k \hat{\gamma}_k^\dagger \left[(\cos(k) - g) v_k^2 - \gamma \sin(k) u_k v_k \right] \quad (16)$$

$$- i \hat{\gamma}_k \hat{\gamma}_{-k} \left[\gamma \sin(k) (u_k^2 - v_k^2) + 2 (\cos(k) - g) u_k v_k \right]$$

$$- i \hat{\gamma}_k^\dagger \hat{\gamma}_{-k}^\dagger \left[\gamma \sin(k) (u_k^2 - v_k^2) + 2 (\cos(k) - g) u_k v_k \right] + g.$$

144 The terms proportional to $\hat{\gamma}_k^\dagger \hat{\gamma}_{-k}^\dagger$ and $\hat{\gamma}_k \hat{\gamma}_{-k}$ should vanish for the Hamiltonian to acquire a diagonal
 145 form. Writing $u_k = \cos(\vartheta_k/2)$ and $v_k = \sin(\vartheta_k/2)$, the Bogoliubov angles satisfy

$$\tan(\vartheta_k) = \frac{\gamma \sin(k)}{g - \cos(k)}. \quad (17)$$

146 For numerical simulations, the last condition can be rewritten as $\gamma \sin(k) \{u_k^2 - v_k^2\} + 2(\cos(k) - g) u_k v_k =$
 147 0. Finally, the Hamiltonian (13) can be rewritten as a sum of noninteracting terms

$$\begin{aligned}\hat{H}^+(g, \gamma) &= \sum_{k \in \mathbf{k}^+} \epsilon_k(g, \gamma) (\hat{n}_k + \hat{n}_{-k} - 1), \\ \hat{H}^-(g, \gamma) &= \sum_{k \in \mathbf{k}^-} \epsilon_k(g, \gamma) (\hat{n}_k + \hat{n}_{-k} - 1) + (g-1)(2\hat{n}_0 - 1) + (g+1)(2\hat{n}_\pi - 1),\end{aligned}\quad (18)$$

148 with $\hat{n}_k = \hat{\gamma}_k^\dagger \hat{\gamma}_k$ denoting the fermion number operator and $\epsilon_k(g, \gamma) = 2\sqrt{(g - \cos k)^2 + \gamma^2 \sin^2 k}$
 149 being the quasiparticle energy of mode $\mathbf{k} \neq 0, \pi$ per particle.

150 2.1 Mathematical tools for the complete Hilbert space

151 To simplify the presentation, we focus on the positive-parity subspace in this subsection. However,
 152 the methods presented are applicable in the negative-parity sector too. In order to keep the notation
 153 clear, we use the following conventions:

- 154 • **Hilbert spaces** are denoted by letters in blackboard bold style, for example \mathbb{H}_k .
- 155 • **Operators** are denoted by letters with a hat, such as \hat{O}_k and \hat{h}_{k_i} .
- 156 • **Operations** on tensor products of Hilbert spaces are denoted with calligraphic letters \mathcal{P} and
 157 \mathcal{N} .

158 To begin with, we note that the positive-parity Hilbert subspace \mathbb{H}^+ can be written as the tensor
 159 product of subspaces corresponding to each *pair of momenta* (k and $-k$)

$$\mathbb{H}^+ = \bigotimes_{k \in \mathbf{k}^+} \mathbb{H}_k. \quad (19)$$

160 Each subspace \mathbb{H}_k is the linear span of the vacuum and states involving one and two Fermionic
 161 excitations with a given momentum

$$\begin{aligned}\mathbb{H}_k &= \text{span}\{|0\rangle_k, \hat{c}_k^\dagger \hat{c}_{-k}^\dagger |0\rangle_k, \hat{c}_k^\dagger |0\rangle_k, \hat{c}_{-k}^\dagger |0\rangle_k\} \\ &= \{|00\rangle_k, |11\rangle_k, |10\rangle_k, |01\rangle_k\}, \quad \forall k \in \mathbf{k}^+.\end{aligned}\quad (20)$$

162 Here, $|0\rangle_k$ is the vector annihilated by both \hat{c}_k and \hat{c}_{-k} . Each of the subspaces can be divided into
 163 the sectors with even $\mathbb{H}_k^{(p)}$ and odd $\mathbb{H}_k^{(n)}$ number of excitations

$$\begin{aligned}\mathbb{H}_k^{(p)} &= \text{span}\{|0\rangle_k, \hat{c}_k^\dagger \hat{c}_{-k}^\dagger |0\rangle_k\} = \{|00\rangle_k, |11\rangle_k\}, \\ \mathbb{H}_k^{(n)} &= \text{span}\{\hat{c}_{-k}^\dagger |0\rangle_k, \hat{c}_k^\dagger |0\rangle_k\} = \{|01\rangle_k, |10\rangle_k\}.\end{aligned}\quad (21)$$

164 Note that the dimension of the right hand side of equation (19) is equal to $4^{L/2} = 2^L$, as there are
 165 $L/2$ positive momenta and each corresponding subspace is four-dimensional. However, there is
 166 an additional condition in the positive-parity subspace: the parity operator $\hat{\Pi}$ has eigenvalue $+1$.
 167 Thus, the subspace is only spanned by vectors associated with an even number of quasiparticles.
 168 We denote this subspace by $\mathcal{P}\left(\bigotimes_{k \in \mathbf{k}^+} \mathbb{H}_k\right)$

$$\mathcal{P} = \mathcal{P}\left(\bigotimes_{k \in \mathbf{k}^+} \mathbb{H}_k\right) = \text{span}\left\{\bigotimes_{k \in \mathbf{k}^+} |i_k j_k\rangle : i_k, j_k \in \{0, 1\}, \sum_{k \in \mathbf{k}^+} (i_k + j_k) \text{ is even}\right\}. \quad (22)$$

169 Similarly, we define the subspace spanned by odd number of quasi-particle excitations and denote
 170 it by $\mathcal{N} = \mathcal{N}\left(\bigotimes_{k \in \mathbf{k}^+} \mathbb{H}_k\right)$. It is easy to see that both spaces $\mathcal{P}\left(\bigotimes_{k \in \mathbf{k}^+} \mathbb{H}_k\right)$ and $\mathcal{N}\left(\bigotimes_{k \in \mathbf{k}^+} \mathbb{H}_k\right)$
 171 have dimension 2^{L-1} and satisfy

$$\mathbb{H}^+ = \mathcal{P}\left(\bigotimes_{k \in \mathbf{k}^+} \mathbb{H}_k\right) \oplus \mathcal{N}\left(\bigotimes_{k \in \mathbf{k}^+} \mathbb{H}_k\right). \quad (23)$$

172 For the positive-parity subspace only \mathcal{P} is relevant; vectors in \mathcal{N} have no physical meaning for
 173 the system described by the Hamiltonian \hat{H}^+ . However, the spaces \mathcal{P} and \mathcal{N} (defined for proper
 174 momenta) exchange their roles for \hat{H}^- ; see Eq. (18). These considerations suggest that to obtain
 175 correct results in the positive-parity subspace, it is sufficient to redefine the tensor product to take
 176 into account only vectors from \mathcal{P} . This can be done for states and observables. Before dealing with
 177 observables, we introduce an alternative recursive definition of the spaces \mathcal{P} and \mathcal{N} , equivalent
 178 to Eq. (22). We shall make use of it in deriving the exact partition function and characteristic
 179 functions of observables. We start by defining the subspaces for one momentum, see Eq. (21),

$$\mathcal{P}(\mathbb{H}_{k_1}) = \mathbb{H}_{k_1}^{(p)}, \quad \mathcal{N}(\mathbb{H}_{k_1}) = \mathbb{H}_{k_1}^{(n)}. \quad (24)$$

180 Next, we specify how to construct spaces \mathcal{P} and \mathcal{N} when a mode with momentum k_{n+1} is added:

$$\begin{aligned} \mathcal{P}\left(\bigotimes_{i=1}^{n+1} \mathbb{H}_{k_i}\right) &= \mathcal{P}\left(\bigotimes_{i=1}^n \mathbb{H}_{k_i}\right) \otimes \mathbb{H}_{k_{n+1}}^{(p)} \oplus \mathcal{N}\left(\bigotimes_{i=1}^n \mathbb{H}_{k_i}\right) \otimes \mathbb{H}_{k_{n+1}}^{(n)}, \quad n \geq 1, \\ \mathcal{N}\left(\bigotimes_{i=1}^{n+1} \mathbb{H}_{k_i}\right) &= \mathcal{N}\left(\bigotimes_{i=1}^n \mathbb{H}_{k_i}\right) \otimes \mathbb{H}_{k_{n+1}}^{(p)} \oplus \mathcal{P}\left(\bigotimes_{i=1}^n \mathbb{H}_{k_i}\right) \otimes \mathbb{H}_{k_{n+1}}^{(n)}, \quad n \geq 1. \end{aligned} \quad (25)$$

181 The intuitive meaning of these equations is that in order to obtain an even number of excitations
 182 one has to add an even number of excitations to an even number, or an odd number of excitations
 183 to an odd number.

184

185 We can extend these definitions for operators and density matrices. We assume that operators
 186 \hat{O}_k act independently on each subspace \mathbb{H}_k and each \hat{O}_k can be written as a sum of an even part
 187 $\hat{O}_k^{(p)}$ and an odd part $\hat{O}_k^{(n)}$ as

$$\hat{O}_k = \hat{O}_k^{(p)} + \hat{O}_k^{(n)}, \quad \hat{O}_k^{(p)} \Big|_{\mathbb{H}_k^{(n)}} = 0, \quad \hat{O}_k^{(n)} \Big|_{\mathbb{H}_k^{(p)}} = 0. \quad (26)$$

188 The operators $\hat{O}_k^{(p)}$ and $\hat{O}_k^{(n)}$ act on the total space \mathbb{H}_k , but have a 2×2 zero block 0_2 in the respective
 189 subspace. The proper restrictions of the tensor product of operators \hat{O}_k can be defined in a similar
 190 way as in Eqs. (24) and (25) for $\mathcal{P}(\hat{O}_{k_1}) = \hat{O}_{k_1}^{(p)}$ and $\mathcal{N}(\hat{O}_{k_1}) = \hat{O}_{k_1}^{(n)}$, and are given by

$$\begin{aligned} \mathcal{P}\left(\bigotimes_{i=1}^{n+1} \hat{O}_{k_i}\right) &= \mathcal{P}\left(\bigotimes_{i=1}^n \hat{O}_{k_i}\right) \otimes \hat{O}_{k_{n+1}}^{(p)} + \mathcal{N}\left(\bigotimes_{i=1}^n \hat{O}_{k_i}\right) \otimes \hat{O}_{k_{n+1}}^{(n)}, \quad n \geq 1, \\ \mathcal{N}\left(\bigotimes_{i=1}^{n+1} \hat{O}_{k_i}\right) &= \mathcal{N}\left(\bigotimes_{i=1}^n \hat{O}_{k_i}\right) \otimes \hat{O}_{k_{n+1}}^{(p)} + \mathcal{P}\left(\bigotimes_{i=1}^n \hat{O}_{k_i}\right) \otimes \hat{O}_{k_{n+1}}^{(n)}, \quad n \geq 1. \end{aligned} \quad (27)$$

Example 2.1: Even and odd parity parts of the Hamiltonian

For \hat{H}_k given by Eq. (14), note that for a each mode k_n the Hamiltonian can be rewritten as

$$\hat{H}_k = \mathcal{P}\left(\hat{\mathbb{I}}_{k_1} \otimes \hat{\mathbb{I}}_{k_2} \otimes \dots \otimes \hat{h}_{k_n} \otimes \dots \otimes \hat{\mathbb{I}}_{k_{L/2}}\right),$$

where, in the basis $\{|00\rangle_k, |11\rangle_k, |01\rangle_k, |10\rangle_k\}$,

$$\hat{h}_{k_n} = 2 \begin{pmatrix} \cos(k_n) - g & \gamma \sin(k_n) & 0 & 0 \\ \gamma \sin(k_n) & g - \cos(k_n) & 0 & 0 \\ 0 & 0 & 0 & 0 \\ 0 & 0 & 0 & 0 \end{pmatrix}.$$

Here, $\hat{h}_{k_n}^{(n)}$ is 4×4 zero matrix (with no odd part), and $\hat{h}_{k_n}^{(p)} = \hat{h}_{k_n}$.

191

192 As the odd part of Hamiltonian is zero, the description using ordinary tensor products instead
 193 of over \mathcal{P} is valid for pure states. However, the canonical thermal Gibbs state has a non-vanishing
 194 odd-parity contribution:

Example 2.2: Even and odd-parity contributions to the exact Gibbs state

Consider the part of the thermal Gibbs state corresponding to momentum k :

$$\hat{\rho}_k = \exp(-\beta \hat{h}_k). \quad (28)$$

Using the expression for \hat{h}_k in the the basis $\{|00\rangle_k, |11\rangle_k, |01\rangle_k, |10\rangle_k\}$,

$$\hat{\rho}_k = \exp \left[-2\beta \begin{pmatrix} \cos(k) - g & \gamma \sin(k) \\ \gamma \sin(k) & g - \cos(k) \end{pmatrix} \right] \oplus \mathbb{I}_2. \quad (29)$$

Therefore, the even and odd parts read:

$$\hat{\rho}_k^{(p)} = \exp \left[-2\beta \begin{pmatrix} \cos(k) - g & \gamma \sin(k) \\ \gamma \sin(k) & g - \cos(k) \end{pmatrix} \right] \oplus 0_2, \quad \hat{\rho}_k^{(n)} = 0_2 \oplus \mathbb{I}_2. \quad (30)$$

Using the fact that \hat{h}_k has eigenvalues $\pm \epsilon_k$, we have:

$$\text{Tr}(\hat{\rho}_k^{(p)}) = 2 \cosh(\beta \epsilon_k(g, \gamma)), \quad \text{Tr}(\hat{\rho}_k^{(n)}) = 2. \quad (31)$$

195

196 Next, we state three propositions helpful in calculating the complete and exact expression of
 197 the partition function and the full counting statistics of observables:

Proposition 2.3: Identities for product of operators

Consider two operators \hat{O}_k and \hat{R}_k acting independently on each subspace \mathbb{H}_k . Then, the following identities are true for operator multiplication

$$\begin{aligned} \mathcal{P} \left(\bigotimes_{i=1}^n \hat{O}_{k_i} \right) \mathcal{P} \left(\bigotimes_{i=1}^n \hat{R}_{k_i} \right) &= \mathcal{P} \left(\bigotimes_{i=1}^n \hat{O}_{k_i} \hat{R}_{k_i} \right), \\ \mathcal{N} \left(\bigotimes_{i=1}^n \hat{O}_{k_i} \right) \mathcal{N} \left(\bigotimes_{i=1}^n \hat{R}_{k_i} \right) &= \mathcal{N} \left(\bigotimes_{i=1}^n \hat{O}_{k_i} \hat{R}_{k_i} \right). \end{aligned} \quad (32)$$

198

199 The following proposition is useful in calculations involving Gibbs states and time-evolutions:

Proposition 2.4: Identities for exponentials of operators

For every set of operators O_k acting on the subspace \mathbb{H}_k , the following identities for exponents of operators hold:

$$\begin{aligned} \exp \left[\mathcal{P} \left(\bigotimes_{i=1}^n \hat{O}_{k_i} \right) \right] &= \mathcal{P} \left(\bigotimes_{i=1}^n \exp(\hat{O}_{k_i}) \right), \\ \exp \left[\mathcal{N} \left(\bigotimes_{i=1}^n \hat{O}_{k_i} \right) \right] &= \mathcal{N} \left(\bigotimes_{i=1}^n \exp(\hat{O}_{k_i}) \right). \end{aligned} \quad (33)$$

200

201 Lastly, the use of traces turns out to be essential to determine expectation values of observables,
 202 and, more generally, their full counting statistics:

Proposition 2.5: Trace identities

Consider operators \hat{O}_k that act independently on each subspace \mathbb{H}_k . Then, the traces of the restricted tensor products can be expressed as follows,

$$\begin{aligned}\mathrm{tr} \left[\mathcal{P} \left(\bigotimes_{i=1}^n \hat{O}_{k_i} \right) \right] &= \frac{1}{2} \left(\prod_{i=1}^n \mathrm{tr}(\hat{O}_{k_i}) + \prod_{i=1}^n (\mathrm{tr}(\hat{O}_{k_i}^{(p)}) - \mathrm{tr}(\hat{O}_{k_i}^{(n)})) \right), \\ \mathrm{tr} \left[\mathcal{N} \left(\bigotimes_{i=1}^n \hat{O}_{k_i} \right) \right] &= \frac{1}{2} \left(\prod_{i=1}^n \mathrm{tr}(\hat{O}_{k_i}) - \prod_{i=1}^n (\mathrm{tr}(\hat{O}_{k_i}^{(p)}) - \mathrm{tr}(\hat{O}_{k_i}^{(n)})) \right).\end{aligned}\tag{34}$$

We present a proof of Eq. (34) in the Appendix A.

203

204 *Negative-parity subspace.* In the negative-parity subspace, all formulas derived for the positive-
205 parity subspace remain valid. In particular, for all momenta $k \neq 0, \pi$ expressions from examples
206 2.1, 2.2 apply. The only difference is that one has to treat carefully the parts of the Hilbert space
207 associated with momenta 0 and π . They are spanned by the following bases:

$$\begin{aligned}\mathbb{H}_0 &= \mathrm{span}\{|0\rangle_0, \hat{c}_0^\dagger |0\rangle_0\}, \\ \mathbb{H}_\pi &= \mathrm{span}\{|0\rangle_\pi, \hat{c}_\pi^\dagger |0\rangle_\pi\}.\end{aligned}\tag{35}$$

208 As a result, matrices describing the Hamiltonian and Gibbs state are 2×2 instead of 4×4 . In the
209 following example we give formulas for the even- and odd-parity parts of the Gibbs state in modes
210 $k = 0, \pi$:

Example 2.6: Even- and odd-parity parts of the exact Gibbs state for 0, π momenta

Using equation (16), the explicit form of the Gibbs state of the modes with momenta 0, π , in the bases $\{|0\rangle_0, \hat{c}_0^\dagger |0\rangle_0\}, \{|0\rangle_\pi, \hat{c}_\pi^\dagger |0\rangle_\pi\}$, are respectively given by

$$\hat{\rho}_0 = \begin{pmatrix} e^{-\beta(g-1)} & 0 \\ 0 & e^{\beta(g-1)} \end{pmatrix}, \quad \hat{\rho}_\pi = \begin{pmatrix} e^{-\beta(g+1)} & 0 \\ 0 & e^{\beta(g+1)} \end{pmatrix}.\tag{36}$$

Thus, the corresponding even- and odd-parity parts read

$$\hat{\rho}_0^{(p)} = \begin{pmatrix} e^{-\beta(g-1)} & 0 \\ 0 & 0 \end{pmatrix}, \quad \hat{\rho}_\pi^{(p)} = \begin{pmatrix} e^{-\beta(g+1)} & 0 \\ 0 & 0 \end{pmatrix},\tag{37a}$$

$$\hat{\rho}_0^{(n)} = \begin{pmatrix} 0 & 0 \\ 0 & e^{\beta(g-1)} \end{pmatrix}, \quad \hat{\rho}_\pi^{(n)} = \begin{pmatrix} 0 & 0 \\ 0 & e^{\beta(g+1)} \end{pmatrix}.\tag{37b}$$

211

212 In closing this section, we point out that when L is odd, the momenta 0 and π appear in the
213 positive-parity subspace; the general formulas (24) and (26) are always valid.

3 The Canonical Partition Function

214 The partition function is a fundamental object in statistical mechanics from which all equilibrium
215 thermal properties of a system can be derived. It further facilitates the study of critical phenomena
216 through the study of its zeroes in the complex plane, known as Lee-Yang zeros [72].
217

218

219 For its study, we consider a linear spin-1/2 chain described by Eq. (1). The system is prepared
220 in a canonical thermal Gibbs state at finite inverse temperature β and characterized by the initial

221 density operator

$$\hat{\rho}_{\text{Gibbs}}(\beta, g, \gamma) = \frac{\exp(-\beta \hat{H}(g, \gamma))}{Z(\beta, g, \gamma)}, \quad (38)$$

222 where $Z(\beta, g, \gamma)$ is the canonical partition function given by

$$Z(\beta, g, \gamma) = \text{tr} \left[\exp(-\beta \hat{H}(g, \gamma)) \right]. \quad (39)$$

223 In a Gibbs state, the system is in a mixture of positive- and negative-parity states and both sub-
 224 spaces should be taken into account. To this end, we consider the operator $\hat{\rho} = \exp(-\beta \hat{H})$, where
 225 \hat{H} is given by Eq. (1). According to the exact diagonalization (see Sec. 2), the total Hamiltonian
 226 can be mapped to a set of independent mode operators in each parity sector. For fixed even L , the
 227 operator $\hat{\rho}$ is given by

$$\hat{\rho} = \exp \left[-\beta (\hat{H}^+ \hat{\Pi}^+ + \hat{H}^- \hat{\Pi}^-) \right] = \hat{\rho}^+ \oplus \hat{\rho}^-, \quad (40)$$

228 where

$$\hat{\rho}^+ = \mathcal{P} \left(\bigotimes_{k \in \mathbf{k}^+} \hat{\rho}_k \right), \quad \hat{\rho}^- = \mathcal{N} \left(\bigotimes_{k \in \mathbf{k}^-} \hat{\rho}_k \otimes \hat{\rho}_0 \otimes \hat{\rho}_\pi \right), \quad (41)$$

229 and $\hat{\rho}_k$ are defined in Examples 2.2, with the sets \mathbf{k}^+ and \mathbf{k}^- given in Eq. (12). For these operators
 230 the corresponding reduced partition functions are

$$Z^+(\beta, g, \gamma) = \text{tr} \left[\mathcal{P} \left(\bigotimes_{k \in \mathbf{k}^+} \hat{\rho}_k \right) \right], \quad \text{and} \quad Z^-(\beta, g, \gamma) = \text{tr} \left[\mathcal{N} \left(\bigotimes_{k \in \mathbf{k}^-} \hat{\rho}_k \otimes \hat{\rho}_0 \otimes \hat{\rho}_\pi \right) \right]. \quad (42)$$

231 For simplicity, we calculate Z^+ and Z^- separately, and focus on Z^+ first. Using the formulas from
 232 Example 2.2, one finds

$$\begin{aligned} \text{tr}(\hat{\rho}_k) &= 2 \cosh(\beta \epsilon_k) + 2 = 4 \cosh^2 \left(\frac{\beta \epsilon_k}{2} \right), \\ \text{tr}(\hat{\rho}_k^{(p)}) - \text{tr}(\hat{\rho}_k^{(n)}) &= 2 \cosh(\beta \epsilon_k) - 2 = 4 \sinh^2 \left(\frac{\beta \epsilon_k}{2} \right). \end{aligned} \quad (43)$$

233 Making use of the first identity in (34), we obtain an expression for canonical partition function
 234 in the positive-parity sector

$$Z^+(\beta, g, \gamma) = \frac{1}{2} \left(\prod_{k \in \mathbf{k}^+} 2^2 \cosh^2 \left(\frac{\beta}{2} \epsilon_k(g, \gamma) \right) + \prod_{k \in \mathbf{k}^+} 2^2 \sinh^2 \left(\frac{\beta}{2} \epsilon_k(g, \gamma) \right) \right). \quad (44)$$

235 The computation of the negative-parity part of the partition function proceeds in the same way; we
 236 use the second of the trace identities (34) and the expressions from the example 2.1 to find

$$\begin{aligned} Z^-(\beta, g, \gamma) &= \frac{1}{2} \left(2^2 \cosh(\beta(g+1)) \cosh(\beta(g-1)) \prod_{k \in \mathbf{k}^-} 2^2 \cosh^2 \left(\frac{\beta}{2} \epsilon_k(g, \gamma) \right) \right. \\ &\quad \left. - 2^2 \sinh(\beta(g+1)) \sinh(\beta(g-1)) \prod_{k \in \mathbf{k}^-} 2^2 \sinh^2 \left(\frac{\beta}{2} \epsilon_k(g, \gamma) \right) \right). \end{aligned} \quad (45)$$

237 Using (40), the exact partition is the sum of contributions of positive and negative parity: $Z(\beta, g, \lambda) =$
 238 $Z^+(\beta, g, \gamma) + Z^-(\beta, g, \gamma)$. To sum up, one can rewrite exact partition function in closed-form.

Summary 3.1: Exact partition function for spin- $\frac{1}{2}$ XY model

$$\begin{aligned}
 Z(\beta, g, \gamma) = & \frac{1}{2} \left(\prod_{k \in \mathbf{K}^+} 2 \cosh\left(\frac{\beta}{2} \epsilon_k(g, \gamma)\right) + \prod_{k \in \mathbf{K}^+} 2 \sinh\left(\frac{\beta}{2} \epsilon_k(g, \gamma)\right) \right. \\
 & \left. + \prod_{k \in \mathbf{K}^-} 2 \cosh\left(\frac{\beta}{2} \epsilon_k(g, \gamma)\right) - \prod_{k \in \mathbf{K}^-} 2 \sinh\left(\frac{\beta}{2} \epsilon_k(g, \gamma)\right) \right), \quad (46)
 \end{aligned}$$

where

$$\epsilon_k(g, \gamma) = 2 \sqrt{(g - \cos(k))^2 + (\gamma \sin(k))^2}, \quad \epsilon_{k=0} = 2(g-1), \quad \epsilon_{k=\pi} = 2(g+1). \quad (47)$$

239

240 In this expression the products run over *all momenta*, not only those with non-negative values.
 241 In general, the total partition function can be represented as the sum of four contributions,

$$Z(\beta, g, \gamma) = \frac{1}{2} \left[Z_F^+(\beta, g, \gamma) + Z_F^-(\beta, g, \gamma) + Z_B^+(\beta, g, \gamma) - Z_B^-(\beta, g, \gamma) \right] \quad (48)$$

242 where $Z_F^\pm(\beta, g, \gamma) = \prod_{k \in \mathbf{K}^\pm} 2 \cosh(\beta \epsilon_k(g, \gamma)/2)$ and $Z_B^\pm(\beta, g, \gamma) = \prod_{k \in \mathbf{K}^\pm} 2 \sinh(\beta \epsilon_k(g, \gamma)/2)$ are
 243 the ‘‘Fermionic’’ and ‘‘boundary’’ contributions. The first term, which takes only into account
 244 Fermionic and positive-parity contribution is the only term considered in the PPA, widely used in
 245 the literature as the correct approximation in the limit $N \rightarrow \infty$ [1, 44, 59, 60, 62, 64]

Summary 3.2: PPA partition function

$$Z_{\text{PPA}}(\beta, g, \gamma) = Z_F^+(\beta, g, \gamma) = \prod_{k \in \mathbf{K}^+} 2 \cosh\left(\frac{\beta}{2} \epsilon_k(g, \gamma)\right). \quad (49)$$

246

247 In the isotropic case with $\gamma = 0$, the exact partition function admits a more compact expres-
 248 sion [73] but this limit lies outside the Ising universality class, our primary focus. The complete
 249 expression for the partition function 3.1 was first derived with the aid of creation and annihilation
 250 operators by Katsura [63]. An alternative approach has been reported using Grassmann variables,
 251 without a numerical characterization [65]; see as well [45].

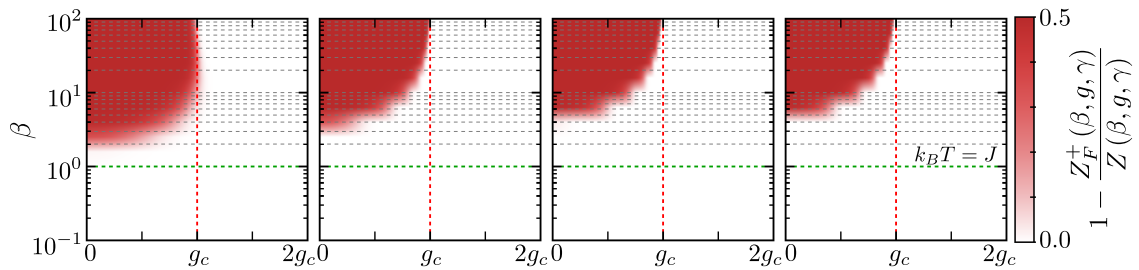


Figure 1: **Comparison of the exact and PPA canonical partition functions.** The ratio between the total partition function 3.1 and the PPA Eq. (49) is shown in the β - g plane for finite system size $L = 50, 100, 5000, 10000$, increasing from left to right (anisotropic parameter $\gamma = 1$). Significant differences appear close to the critical point $g = g_c = 1$, with the magnitude of $Z_F^+(\beta, g, \gamma)$ deviating by 50% from the exact partition function. The paramagnetic phase is correctly reproduced by the simplified approximation $g > g_c$ while errors in the partition function are shown in red in the ferromagnetic phase at low temperatures.

252 It is thus natural to analyze the extent to which the PPA $Z_F^+(\beta, g, \gamma)$ provides a valid approxi-
 253 mation to the exact partition function.

254 Fig. 1 shows the difference between the ratio $Z_F^+(\beta) / Z(\beta)$ as a function of the inverse of tempera-
 255 ture and the magnetic field. The error is negligible away from criticality and at high temperatures.
 256 However, prominent discrepancies between the exact partition function (48) and the ubiquitously-
 257 used PPA (49) are manifested in the neighborhood of the critical point in the regime of low-
 258 temperatures, which is often times the regime studied and of interest. Indeed, in this region errors
 259 reach sufficiently large values such that $Z_F^+(\beta, g, \gamma) \approx 0.5 Z(\beta, g, \gamma)$.

260 One can provide a simple and intuitive explanation of the magnitude of this discrepancy by
 261 considering the structure of the spectrum. The complete spectrum consists of two disjoint “lad-
 262 ders” of levels, spanning the positive-parity and negative-parity subspaces. In the following anal-
 263 ysis we denote by E_g^α and $|g^\alpha\rangle$ the lowest energy level and the corresponding eigenstate in the
 264 subspace of parity $\alpha = \pm$. The diagonalization procedure of the Ising model yields explicit formu-
 265 las for these eigenvalues. For even number of spins [74]

$$\begin{aligned} E_g^+ &= - \sum_{k \in \mathbf{k}^+} \epsilon_k, \\ E_g^- &= - \sum_{k \in \mathbf{k}^-} \epsilon_k - 2. \end{aligned} \quad (50)$$

266 The corresponding eigenstates read

$$\begin{aligned} |g^+\rangle &= \prod_{k \in \mathbf{k}^+} (\cos(\vartheta_k/2) - \sin(\vartheta_k/2) \hat{c}_k^\dagger \hat{c}_{-k}^\dagger) |\text{vac}\rangle, \\ |g^-\rangle &= c_0^\dagger \prod_{k \in \mathbf{k}^-} (\cos(\vartheta_k/2) - \sin(\vartheta_k/2) \hat{c}_k^\dagger \hat{c}_{-k}^\dagger) |\text{vac}\rangle, \end{aligned} \quad (51)$$

267 where $|\text{vac}\rangle$ is annihilated by all \hat{c}_k for $k \in \mathbf{K}^+ \cup \mathbf{K}^-$ (including 0 and π modes). In what follows,
 268 we restrict ourselves to the TFQIM ($\gamma = 1$). In the TFQIM with even number of spins L , the true
 269 ground state always lies in the positive-parity subspace (this is not necessary true in the XY model,
 270 see [75]). The energy gap $\delta(g)$ between these two lowest energy states plays a crucial role. We
 271 recall its asymptotic behavior [74]

$$\begin{aligned} \delta(0 < g < 1) &= \mathcal{O}[\sim \exp(-L/\xi(g))], \\ \delta(g = 1) &= 2 \tan\left[\frac{\pi}{4L}\right] \approx \frac{\pi}{2L}, \\ \delta(g > 1) &= 2g - 2 + \mathcal{O}(g^{-L}), \end{aligned} \quad (52)$$

272 where $\xi(g)$ denotes the correlation length. In the low temperature regime, the Gibbs state is ef-
 273 fectively spanned by the two lowest energy states, $|g^+\rangle$ and $|g^-\rangle$. In this truncation, the partition
 274 function and Gibbs state read

$$Z_{\text{approx}}(\beta, g) = e^{-\beta E_g^+} + e^{-\beta E_g^-}, \quad (53)$$

275

$$\rho_{\text{Gibbs}}(\beta, g) \approx \frac{1}{Z_{\text{approx}}(\beta, g)} \left(e^{-\beta E_g^+} |g^+\rangle \langle g^+| + e^{-\beta E_g^-} |g^-\rangle \langle g^-| \right). \quad (54)$$

276 This low-temperature two-level approximation relies on (51) and disregards the contribution from
 277 higher excited states, that are energetically separated from $|g^+\rangle$ and $|g^-\rangle$. The energy gap to the next
 278 excited state can be calculated as the energy of a single-particle excitation in the positive-parity
 279 subspace, which sufficiently far from the critical point is estimated by

$$\Delta(g) = 4 \sqrt{g^2 - 2g \cos\left(\frac{\pi}{L}\right) + 1} = 4|g - 1| + \mathcal{O}\left(\frac{1}{L^2}\right), \quad g > 0, g \neq 1, \quad (55)$$

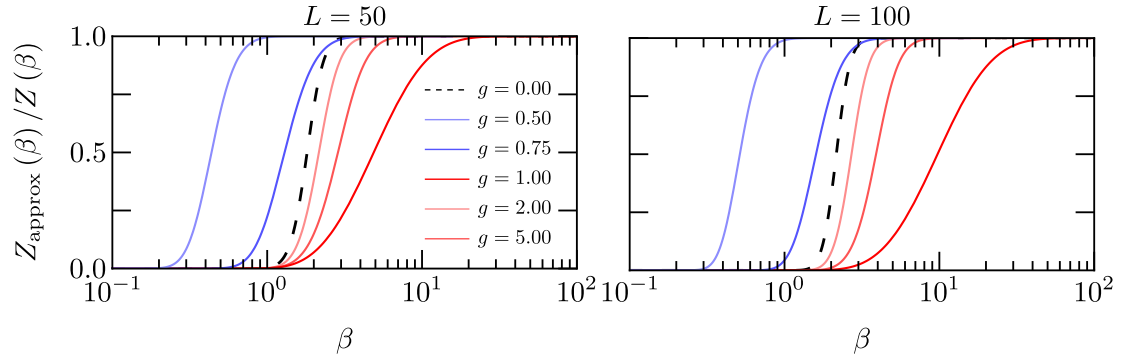


Figure 2: Ratio between the low-temperature approximation and exact partition functions as a function of the inverse temperature. The accuracy of the two-level approximation (53) is considered for different values of the transverse magnetic field g and two different system sizes. As the energy gaps $\delta(g)$ and $\Delta(g)$ in the neighbourhood of $g_c = 1$ are comparable, a lower temperature is required to obtain a desired level of accuracy. For given β , the accuracy decreases with increasing system size.

280 while at the critical point, this gap behaves as

$$\Delta(g = 1) \approx \frac{4\pi}{L}. \quad (56)$$

281 In the ferromagnetic phase, the first excited state is separated from the ground state by an expo-
 282 nentially vanishing gap and the second excited state lies far away from both of them. Therefore,
 283 the correction from high-energy states is negligible in the low temperature limit $\beta\Delta(g) \gg 1$. Simi-
 284 larly, in the paramagnetic phase, the ground state is energetically separated from all the excited
 285 states. At the critical point the two lowest excited states are separated from the ground state by a
 286 comparable gap,

$$\frac{\Delta(g = 1)}{\delta(g = 1)} \xrightarrow{L \rightarrow \infty} \frac{1}{8}. \quad (57)$$

287 However, for large β the error is very small. The accuracy of the the two-level approximation for
 288 different phases is shown in Fig. 2. The validity of this approximation (53) explains the magnitude
 289 of the errors between the exact and the PPA partition functions shown in Fig. 1. For $g < 1$, the
 290 simplified partition function takes into account only the ground state $|g^+\rangle$ and can be approximated
 291 by $e^{-\beta E_g^+}$, while the complete partition function is approximately

$$Z_{\text{approx}}(\beta, g) \approx e^{-\beta E_g^+} + e^{-\beta E_g^-} \approx 2e^{-\beta E_g^+}. \quad (58)$$

292 This explains the observed error of about 50% between the exact and PPA partition functions.

293 4 Full Counting Statistics in Integrable Spin Chains

294 The characterization of a given observable in a quantum system generally relies on the study of its
 295 expectation value. To determine it, experiments often collect a number of measurements, and build
 296 a histogram, from which the eigenvalue distribution is estimated. The full counting statistics of an
 297 observable focuses on the complete eigenvalue distribution. Its study has proved useful in a wide
 298 variety of applications and alternative methods for its measurement have been put forward [76]. A
 299 prominent example concerns the counting statistics of the number of fermions (electrons) travers-
 300 ing a point contact in a wire, that is described by the Levitov-Lesovik formula [77–79]. Dis-
 301 tributions of other observables such as the total energy play a key role in quantum chaos [80]

302 and the statistics of related positive-operator valued measures (POVMs, such as work) are at the
 303 core of fluctuation theorems in quantum thermodynamics [81]. In the context of spin chains, the
 304 distribution of the order parameter has long been recognized as a probe for criticality and turbu-
 305 lence [82–90]. Further, the study of the full counting statistics of quasiparticles and topological
 306 defects has been key to uncover universal dynamics of phase transitions beyond the paradigmatic
 307 Kibble-Zurek mechanism [16, 27–30, 91].

308
 309 The full counting statistics is characterized by the probability $P(\omega)$ to obtain the eigenvalue ω
 310 of a general operator \hat{W} . It is defined as the expectation value

$$P(\omega) = \left\langle \delta(\hat{W} - \omega) \right\rangle, \quad (59)$$

311 where the δ function is to be interpreted as a Kronecker or Dirac delta function, depending on
 312 whether the spectrum of \hat{W} is point-wise or continuous. The angular bracket denotes the quantum
 313 expectation value with respect to a general state characterized by a density matrix $\hat{\rho}$. We introduce
 314 the Fourier transform representation

$$P(\omega) = \frac{1}{2\pi} \int_{-\infty}^{\infty} d\theta \tilde{P}(\theta) \exp(-i\theta\omega), \quad (60)$$

315 where $\tilde{P}(\theta)$ is the characteristic function given by

$$\tilde{P}(\theta) = \text{tr} \left[\hat{\rho} \exp(i\theta\hat{W}) \right]. \quad (61)$$

316 In cases such as the kink number and the transverse magnetization, the eigenvalues are integers
 317 $\omega \in \mathbb{Z}$ and the range of the integral can be restricted from $-\pi$ to π . The characteristic function is
 318 also known as the moment generating function, as it allows to directly compute the mean value
 319 and higher-order moments of a given observable \hat{W} according to

$$\langle \hat{W}^m \rangle = \frac{1}{i^m} \frac{d^m}{d\theta^m} \tilde{P}(\theta) \Big|_{\theta=0}. \quad (62)$$

320 Further, its logarithm is the cumulant generating function used to derive the cumulants of the
 321 distribution through the identity

$$\kappa_m = (-i)^m \frac{d^m}{d\theta^m} \ln \tilde{P}(\theta) \Big|_{\theta=0}. \quad (63)$$

322 The first cumulant κ_1 is just the mean value, κ_2 is the variance, and κ_3 coincides with the third
 323 central moment. Cumulants are useful in characterizing fluctuations in a quantum system. For
 324 example, since the only distribution with finite $\kappa_1, \kappa_2 \neq 0$ and vanishing $\kappa_m = 0$ for $m > 2$ is the
 325 Gaussian distribution, higher cumulants quantify non-normal features of the distribution of inter-
 326 est, e.g., an eigenvalue distribution.

327
 328 We next derive the general form of characteristic function for a wide class \mathcal{W} of observables.
 329 This class is defined by the property that any operator $\hat{W} \in \mathcal{W}$, in each parity subspace, can be
 330 written in the form

$$\hat{W} = \sum_k \hat{W}_k, \quad (64)$$

331 where

$$\hat{W}_k = \hat{\Psi}_k^\dagger \hat{w}_k \hat{\Psi}_k, \quad \hat{\Psi}^\dagger = (\hat{c}_{-k}, \hat{c}_k^\dagger, \hat{c}_k, \hat{c}_{-k}^\dagger) \quad (65)$$

332 and the matrix \hat{w}_k has the block-diagonal form

$$\hat{w}_k = \begin{pmatrix} \hat{w}_k^{(1)} & 0 \\ 0 & \hat{w}_k^{(2)} \end{pmatrix}. \quad (66)$$

333 Here, $\hat{w}_k^{(1)}$ and $\hat{w}_k^{(2)}$ are 2×2 are matrices for momenta different from $0, \pi$ and 1×1 matrices for $0, \pi$
 334 momenta. We point out that the notation in equations (65, 66) is compatible with matrix expres-
 335 sions from Examples 2.1, 2.2, written in the basis $\{|00\rangle_k, |11\rangle_k, |01\rangle_k, |10\rangle_k\}$. When off-diagonal
 336 blocks vanish, the operator \hat{W}_k can be written as a quadratic form in Fermionic operators. How-
 337 ever, there are relevant observables which have components linear in Fermionic operators. For
 338 example, the longitudinal magnetizations X_i or Y_i do not belong to the class \mathcal{W} as these observ-
 339 ables mix the subspaces with different parities. This leads to severe difficulties. Namely, one has
 340 to switch between fermionic operators defined for different sets of momenta. For example, for a
 341 given $k \in \mathbf{K}^-$ one has to perform inverse Fourier transform to express c_k as a linear combination
 342 of fermionic operators in space domain, and then apply Fourier transform with \mathbf{K}^+ as a set of
 343 momenta. This will cause, that subspaces with different momenta will be all intertwined, con-
 344 trary to the basic feature exploited in the systems with periodic boundary conditions - that one can
 345 perform calculations independently for every momentum. The treatment of such operators is thus
 346 beyond the scope of this paper. The systematic treatment of longitudinal magnetization in zero
 347 temperature for Ising model with PBC was conducted in [93], with further extensions including
 348 observables involving three fermionic operators in [89]. For other approaches, see for example
 349 [92] (open boundary conditions) or [61] (exploiting methods of field theory).

350

351 In the following we present the detailed procedure for computing characteristic function $\tilde{P}(\theta)$
 352 of a given observable \hat{W} in the class \mathcal{W} .

353 1. First, we fix the state $\hat{\rho}$ to be the thermal-equilibrium Gibbs state, $\hat{\rho} = \hat{\rho}_{\text{Gibbs}}$ given by
 354 equation (38). Then, using formulas from Section 2 we can diagonalize the even-parity part
 355 of $\hat{\rho}_k$

$$\exp \left[-2\beta \begin{pmatrix} \cos(k) - g & \gamma \sin(k) \\ \gamma \sin(k) & g - \cos(k) \end{pmatrix} \right] = \hat{S}_k^\dagger \text{diag} \left(e^{-\beta \epsilon_k(g, \gamma)}, e^{\beta \epsilon_k(g, \gamma)} \right) \hat{S}_k, \quad (67)$$

356 where

$$\hat{S}_k = \begin{pmatrix} \cos\left(\frac{\vartheta_k}{2}\right) & \sin\left(\frac{\vartheta_k}{2}\right) \\ \sin\left(\frac{\vartheta_k}{2}\right) & -\cos\left(\frac{\vartheta_k}{2}\right) \end{pmatrix} \quad (68)$$

357 and the angle ϑ_k satisfies

$$\cos(\vartheta_k) = \frac{2(\cos(k) - g)}{\epsilon_k(g, \gamma)}, \quad \sin(\vartheta_k) = \frac{2\gamma \sin(k)}{\epsilon_k(g, \gamma)}. \quad (69)$$

358 2. As in the case of the partition function, it is convenient to separate in the full characteristic
 359 function the contributions of positive and negative parity:

$$\tilde{P}(\theta) = \frac{1}{Z(\beta, g, \gamma)} \left(\tilde{P}^+(\theta) + \tilde{P}^-(\theta) \right). \quad (70)$$

360 Using Propositions 2.3 and 2.4, we aim at calculating

$$\tilde{P}^+(\theta) = \text{tr} \left[\mathcal{P} \left(\bigotimes_{k \in \mathbf{K}^+} \hat{\rho}_k \exp(i\theta \hat{w}_k) \right) \right], \quad \tilde{P}^-(\theta) = \text{tr} \left[\mathcal{N} \left(\bigotimes_{k \in \mathbf{K}^-} \hat{\rho}_k \exp(i\theta \hat{w}_k) \right) \right]. \quad (71)$$

361 Next, we define the matrix

$$\hat{\sigma}_k = \hat{S}_k \exp(i\theta \hat{w}_k^{(1)}) \hat{S}_k^\dagger. \quad (72)$$

362 Denoting the eigenvalues of $\hat{w}_k^{(2)}$ by μ_k and λ_k we find

$$\begin{aligned} \text{tr} [\hat{\rho}_k \exp(i\theta \hat{w}_k)] &= \hat{\sigma}_k^{11} e^{-\beta \epsilon_k(g, \gamma)} + \hat{\sigma}_k^{22} e^{\beta \epsilon_k(g, \gamma)} + e^{i\theta \mu_k} + e^{i\theta \lambda_k}, \\ \text{tr} [\hat{\rho}_k^{(p)} \exp(i\theta \hat{w}_k^{(p)})] - \text{tr} [\hat{\rho}_k^{(n)} \exp(i\theta \hat{w}_k^{(n)})] &= \hat{\sigma}_k^{11} e^{-\beta \epsilon_k(g, \gamma)} + \hat{\sigma}_k^{22} e^{\beta \epsilon_k(g, \gamma)} - e^{i\theta \mu_k} - e^{i\theta \lambda_k}. \end{aligned} \quad (73)$$

363 Using Proposition 2.5 we obtain

$$2\tilde{P}^+(\theta) = \prod_{k \in \mathbf{k}^+} \left(\hat{\sigma}_k^{11} e^{-\beta \epsilon_k(g, \gamma)} + \hat{\sigma}_k^{22} e^{\beta \epsilon_k(g, \gamma)} + e^{i\theta\mu} + e^{i\theta\lambda} \right) \\ + \prod_{k \in \mathbf{k}^+} \left(\hat{\sigma}_k^{11} e^{-\beta \epsilon_k(g, \gamma)} + \hat{\sigma}_k^{22} e^{\beta \epsilon_k(g, \gamma)} - e^{i\theta\mu} - e^{i\theta\lambda} \right). \quad (74)$$

364 3. To determine $\tilde{P}^-(\theta)$ it remains to compute the contributions corresponding to $0, \pi$ momenta.
365 Denoting

$$\hat{w}_0 = \text{diag}(w_0^1, w_0^2), \quad \hat{w}_\pi = \text{diag}(w_\pi^1, w_\pi^2), \quad (75)$$

366 one finds

$$\hat{\rho}_0 \exp(i\theta \hat{w}_0) = \text{diag}\left(e^{\beta(g-1)+i\theta w_0^1}, e^{-\beta(g-1)+i\theta w_0^2}\right), \\ \hat{\rho}_\pi \exp(i\theta \hat{w}_\pi) = \text{diag}\left(e^{\beta(g+1)+i\theta w_\pi^1}, e^{-\beta(g+1)+i\theta w_\pi^2}\right). \quad (76)$$

367 Therefore, the negative-parity part of the characteristic function is

$$2\tilde{P}^-(\theta) = \tilde{P}^F(\theta) \prod_{k \in \mathbf{k}^-} \left(\hat{\sigma}_k^{11} e^{-\beta \epsilon_k(g, \gamma)} + \hat{\sigma}_k^{22} e^{\beta \epsilon_k(g, \gamma)} + e^{i\theta\mu} + e^{i\theta\lambda} \right) \\ - \tilde{P}^B(\theta) \prod_{k \in \mathbf{k}^-} \left(\hat{\sigma}_k^{11} e^{-\beta \epsilon_k(g, \gamma)} + \hat{\sigma}_k^{22} e^{\beta \epsilon_k(g, \gamma)} - e^{i\theta\mu} - e^{i\theta\lambda} \right), \quad (77)$$

368 where

$$\tilde{P}^F(\theta) = \left(e^{\beta(g-1)+i\theta w_0^1} + e^{-\beta(g-1)+i\theta w_0^2} \right) \left(e^{\beta(g+1)+i\theta w_\pi^1} + e^{-\beta(g+1)+i\theta w_\pi^2} \right), \\ \tilde{P}^B(\theta) = \left(e^{\beta(g-1)+i\theta w_0^1} - e^{-\beta(g-1)+i\theta w_0^2} \right) \left(e^{\beta(g+1)+i\theta w_\pi^1} - e^{-\beta(g+1)+i\theta w_\pi^2} \right). \quad (78)$$

369 Note that this is not the only way to calculate the characteristic function: instead of diagonalizing
370 $\hat{\rho}_k$, one could diagonalize an observable \hat{w}_k . However, in our approach the role of the Boltzmann
371 factor set by $\beta \epsilon_k(g, \gamma)$, which is usually dominant, is clear from the formulas (74) and (77). In
372 the following sections we apply this method to characterize the full counting statistics of two
373 physically important observables, the number of kinks and the transverse magnetization.

374 4.1 Probability distribution of the number of kinks at thermal equilibrium

375 We next derive the full generating function for the kink-number operator, which is of fundamental
376 importance in the study of quantum phase transitions [12, 16, 27–30]. Although the relevance
377 of this operator is most apparent in the Ising model, it is also well-defined for the general XY
378 model. In the following, we consider the TFQIM with $\gamma = 1$ for simplicity. The explicit form of
379 kink-number operator reads

$$\hat{N} = \frac{1}{2} \sum_{n=1}^L (1 - \hat{X}_n \hat{X}_{n+1}), \quad (79)$$

380 with eigenvalues $n = 0, 1, \dots, L$ under periodic boundary conditions.

381 Comparing the Ising Hamiltonian Eq. (1), with $\gamma = 1$ and $g = 0$, with the Bogoliubov Hamil-
382 tonian (18) at $\gamma = 1$ and $g = 0$, the kink operator takes a simple form as the sum of the number
383 operators of quasiparticles in each momentum [12]. Here, we generalize the kink number operator
384 definition for all values of the magnetic field. First, we rewrite the operator (79) in the following
385 form:

$$\hat{N} = \frac{L}{2} + \sum_k \hat{N}_k. \quad (80)$$

386 By analogy with Eq. (65) and Eq. (66), we define a new set of operators \hat{n}_k , \hat{n}_0 , and \hat{n}_π ; taking for
 387 any mode $k \neq 0, \pi$ the basis given by $\{|00\rangle_k, |11\rangle_k, |01\rangle_k, |10\rangle_k\}$, while selecting for $0, \pi$ momenta
 388 the basis $\{|0\rangle_0, c_0^\dagger |0\rangle_0\}, \{|0\rangle_\pi, c_\pi^\dagger |0\rangle_\pi\}$. Therefore, we define the operators

$$\hat{n}_k = \begin{pmatrix} \cos(k) & \sin(k) & 0 & 0 \\ \sin(k) & -\cos(k) & 0 & 0 \\ 0 & 0 & 0 & 0 \\ 0 & 0 & 0 & 0 \end{pmatrix}, \quad \hat{n}_0 = \begin{pmatrix} \frac{1}{2} & 0 \\ 0 & -\frac{1}{2} \end{pmatrix} \quad \hat{n}_\pi = \begin{pmatrix} -\frac{1}{2} & 0 \\ 0 & \frac{1}{2} \end{pmatrix}, \quad (81)$$

389 and thus

$$\hat{n}_k^{(1)} = \begin{pmatrix} \cos(k) & \sin(k) \\ \sin(k) & -\cos(k) \end{pmatrix}, \quad \hat{n}_k^{(2)} = 0_2. \quad (82)$$

390 Note that $\exp(i\theta\hat{n}_k^{(1)})$ has the simple form

$$\exp(i\theta\hat{n}_k^{(1)}) = \begin{pmatrix} \cos(\theta) + i \sin(\theta) \cos(k) & i \sin(\theta) \sin(k) \\ i \sin(\theta) \sin(k) & \cos(\theta) - i \sin(\theta) \cos(k) \end{pmatrix}. \quad (83)$$

391 Using expressions (68) and (72), one finds

$$\begin{aligned} \sigma_k^{11} &= \cos(\theta) + i \sin(\theta) \cos(k - \vartheta_k), \\ \sigma_k^{22} &= \cos(\theta) - i \sin(\theta) \cos(k - \vartheta_k). \end{aligned} \quad (84)$$

392 This yields the explicit expression of the full characteristic function of the kink-number operator.

Summary 4.1: Full characteristic function for kink number operator

The full characteristic function of the kink number operator Eq. (79) at thermal equilibrium reads

$$\tilde{P}(\theta) = \frac{1}{Z(\beta, g, \gamma)} [\tilde{P}^+(\theta) + \tilde{P}^-(\theta)]. \quad (85)$$

Positive part of characteristic function:

$$\begin{aligned} \tilde{P}^+(\theta) &= \frac{\exp(iL\theta/2)}{2} \left[\prod_{k \in \mathbf{k}^+} 2(\cos(\theta) \cosh[\beta\epsilon_k(g, \gamma)] - i \sin(\theta) \sinh[\beta\epsilon_k(g, \gamma)] \cos(k - \vartheta_k) + 1) \right. \\ &\quad \left. + \prod_{k \in \mathbf{k}^+} 2(\cos(\theta) \cosh[\beta\epsilon_k(g, \gamma)] - i \sin(\theta) \sinh[\beta\epsilon_k(g, \gamma)] \cos(k - \vartheta_k) - 1) \right]. \end{aligned} \quad (86)$$

Negative part of characteristic function:

$$\begin{aligned} \tilde{P}^-(\theta) &= \frac{\exp(iL\theta/2)}{2} \left[\tilde{P}^F(\theta) \prod_{k \in \mathbf{k}^-} 2(\cos(\theta) \cosh[\beta\epsilon_k(g, \gamma)] - i \sin(\theta) \sinh[\beta\epsilon_k(g, \gamma)] \cos(k - \vartheta_k) + 1) \right. \\ &\quad \left. - \tilde{P}^B(\theta) \prod_{k \in \mathbf{k}^-} 2(\cos(\theta) \cosh[\beta\epsilon_k(g, \gamma)] - i \sin(\theta) \sinh[\beta\epsilon_k(g, \gamma)] \cos(k - \vartheta_k) - 1) \right], \end{aligned} \quad (87)$$

where

$$\begin{aligned} \tilde{P}^F(\theta) &= 2^2 \cosh\left(\frac{\beta\epsilon_{k=0} + i\theta}{2}\right) \cosh\left(\frac{\beta\epsilon_{k=\pi} - i\theta}{2}\right), \\ \tilde{P}^B(\theta) &= 2^2 \sinh\left(\frac{\beta\epsilon_{k=0} + i\theta}{2}\right) \sinh\left(\frac{\beta\epsilon_{k=\pi} - i\theta}{2}\right). \end{aligned} \quad (88)$$

The exact total partition function is given by Eq. (48), with the eigenenergies $\epsilon_k(g, \gamma)$ and $\epsilon_{k=0}$ given by Eq. (47), and the Bogoliubov angles ϑ_k satisfying Eq. (17).

393

394 By contrast, in the customary PPA, the characteristic function of the kink-number operator in
 395 the thermodynamic limit contains only the first term of $\tilde{P}^+(\theta)$:

396

397

Summary 4.2: PPA characteristic function for kink number

In the thermodynamic limit, Eq. (85) reduces to

$$\tilde{P}_{\text{PPA}}(\theta) = \frac{\exp(iL\theta/2)}{Z_F^+(\beta, g, \gamma)} \prod_{k \in \mathbf{k}^+} 2(\cos(\theta) \cosh(\beta\epsilon_k(g, \gamma)) - i \sin(\theta) \sinh(\beta\epsilon_k(g, \gamma)) \cos(k - \vartheta_k) + 1), \quad (89)$$

where $Z_F^+(\beta, g, \gamma)$ is defined in (49).

398

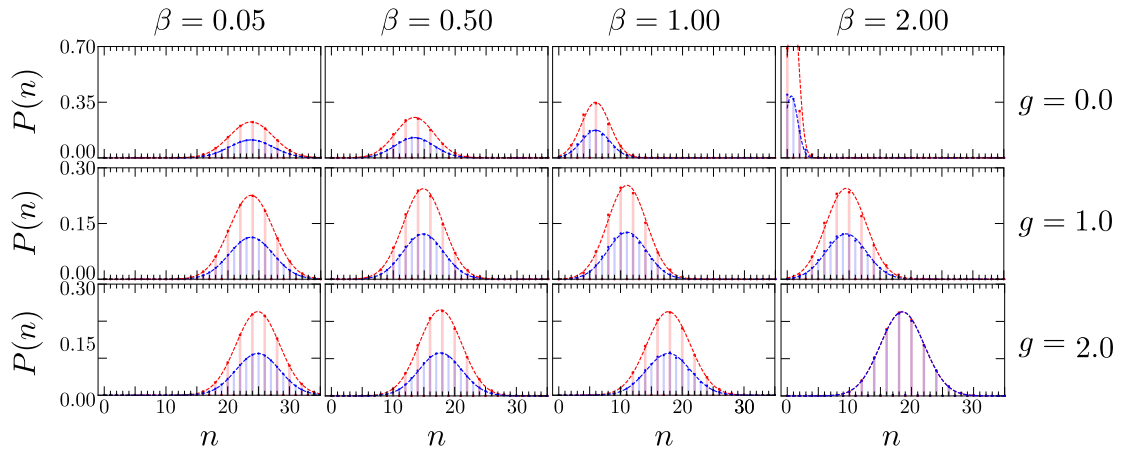


Figure 3: **Kink-number distribution at thermodynamic equilibrium.** Probability distribution of the number of kinks $P(n)$ as a function of the magnetic field g and temperature T for a chain of $L = 50$ spins. The exact probability distribution Eq. (85) (red bars) is compared with the simplified expression in Eq. (89) (blue bars). Only in the low-temperature paramagnet the PPA is accurate. Further, the normal (Gaussian) approximation to the histograms is also shown (dashed lines).

399 In Figure 3, we characterize the full counting statistics of kinks as a function of the magnetic
 400 field and inverse temperature. By numerical integration of Eq. (60), we find the exact probability
 401 distribution function $P(n)$ using Eq. (85). Additionally, we evaluate the PPA probability distribu-
 402 tion function using Eq. (89). The use of the PPA partition functions is widely extended in the liter-
 403 ature, e.g., to analyze the formation of kinks after non-equilibrium quenches [1, 44, 59, 60, 62, 64].
 404 For a large magnetic field and low temperature, the PPA works well and reproduces essentially
 405 the exact full counting statistics of kinks. By contrast, when thermal fluctuations are suppressed
 406 and the magnetic field contribution dominates, the PPA leads to pronounced discrepancies (i.e.
 407 see Fig. 3 lower-left panels). The PPA also fails to account for momentum conservation. Under
 408 periodic boundary conditions, kinks appear in pairs. In general, the PPA incorrectly predicts a
 409 non-zero probability of exciting *odd* number of kinks:

$$P_{\text{PPA}}(n = 2\ell + 1) = \frac{1}{2\pi} \int_{-\pi}^{\pi} d\theta \tilde{P}(\theta) \exp[-i\theta(2\ell + 1)] \neq 0, \quad (90)$$

410 but for large g and β as shown in 3, when $P_{\text{PPA}}(n = 2\ell + 1) \approx 0$.

411 The fact that only even number of kinks in the presence of periodic boundary conditions
 412 can be excited is intuitively clear. For a simple mathematical argument, consider the operator

413 $\prod_{n=1}^L \hat{X}_n \hat{X}_{n+1}$ which is 1 for even kink number and -1 for an odd number. Using $\hat{X}_{L+1} = \hat{X}_1$ and
 414 $(\hat{X}_n)^2 = \otimes_{n=1}^L \hat{I}_n$, it satisfies:

$$\prod_{n=1}^L \hat{X}_n \hat{X}_{n+1} = 1. \quad (91)$$

415 The PPA characteristic function, $\tilde{P}^+(\theta)$ and $\tilde{P}^-(\theta)$ do not exhibit this feature.

416

417 In addition, we note that the magnitude of the exact $P(n)$ for even n can be approximated by
 418 the coarse-grained PPA approximation, whenever the distribution is symmetric, with tails far from
 419 the origin, i.e.,

$$P(n) \approx P_{\text{PPA}}(n) + \frac{1}{2} [P_{\text{PPA}}(n-1) + P_{\text{PPA}}(n+1)], \quad (92)$$

as shown in Figure 4.

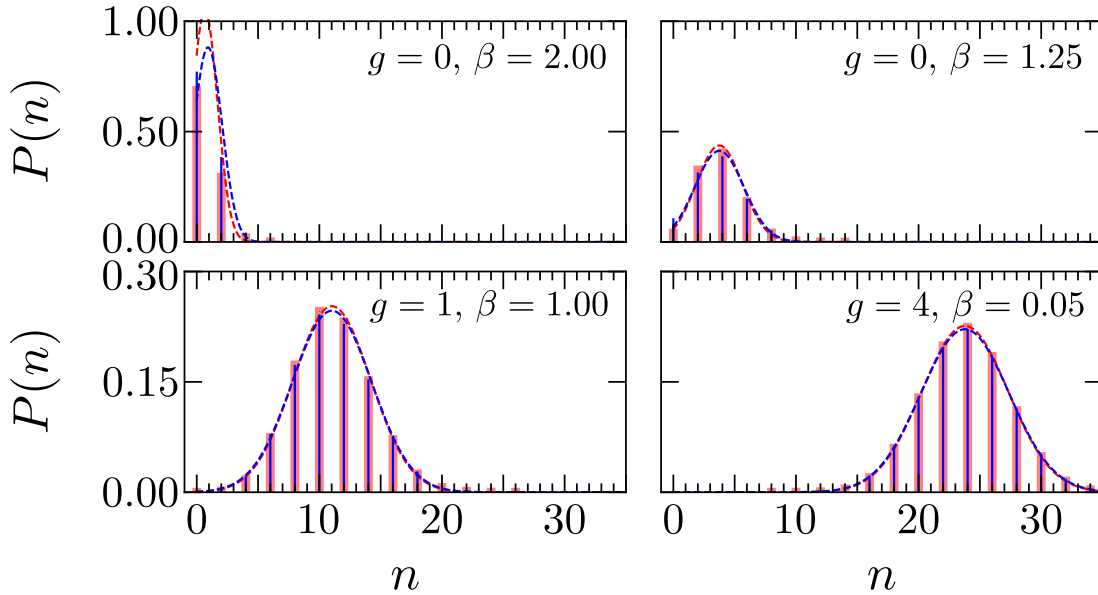


Figure 4: **Exact and Coarse-grained PPA kink-number probability distributions at thermal equilibrium.** The exact kink-number probability distribution evaluated using Eq. (85) (red) is compared with the coarse-grained PPA probability distribution Eq. (92) (blue). The numerical histograms are compared with the Gaussian $N(\kappa_1, \kappa_2)$ with fitted numerical values for κ_1 and κ_2 (dashed lines). In as much as the exact distribution is symmetric and its left tail is negligible near the origin, the coarse-graining of the PPA distribution in Eq. (92) reproduces accurately the exact distribution. Deviations are manifested at low g and temperature, when the distribution is asymmetric.

420

421 An analysis of the cumulants of the kink-number distribution as a function of the inverse
 422 temperature is presented in Fig. 5 for various system sizes. In the paramagnetic phase ($g >$
 423 1), the mean always exceeds the variance, making the kink-number distribution sub-Poissonian.
 424 This need not be the case in the ferromagnetic phase, where the distribution changes from sub-
 425 Poissonian to super-Poissonian as the temperature decreases. This behavior is shown to be robust
 426 as a function of the system size. The difference between the exact cumulant values and those
 427 derived from the PPA is systematically studied in Fig. 6 for a system size of $L = 12$ spins;
 428 the relative error is reduced with increasing system size. The quality of the PPA improves with
 429 increasing temperature, in the classical regime, in the ferromagnetic phase. While the dependence

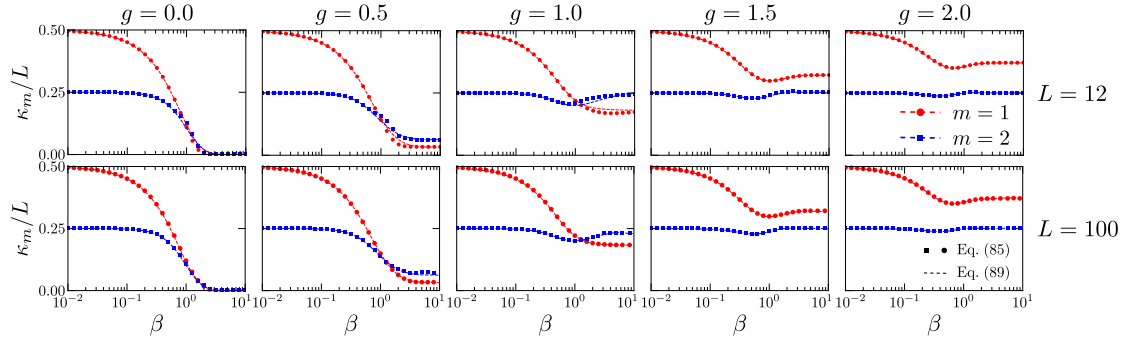


Figure 5: **Cumulants of the kink-number distribution as a function of the inverse of temperature β .** Using the exact characteristic function given by Eq. (85), the mean kink number κ_1 and the variance κ_2 are shown by red circles and blue squares, respectively. The dashed lines correspond to the numerical results using the PPA characteristic function in Eq. (89). While in the paramagnetic phase the statistics is sub-Poissonian, in the ferromagnetic phase it changes from sub- to super-Poissonian as the temperature is decreased. The magnetic field is increased from 0.0 to 2.0, varying from left to right in steps of 0.5. In the upper panels, the system size is $L = 12$, while in the lower ones $L = 100$.

430 of the relative error as a function of the magnetic field g is not monotonic, the bigger discrepancies
 431 between the exact results and the PPA are found in the ferromagnetic phase in the low temperature
 432 regime, when the relative error can reach 100%. In the paramagnetic phase, the PPA provides an
 433 accurate description of the cumulants for different temperatures and values of the magnetic field.

434 To complete the characterization of the kink-number distribution we consider the limiting
 435 cases of the ground-state distribution ($\beta \rightarrow \infty$) and the infinite-temperature case ($\beta \rightarrow 0$) in an
 436 exact approach, without using the PPA. The first can be easily described using (83), while in the
 437 second we consider a maximally-mixed Gibbs state and apply trace formulas 2.5. For $\beta = 0$, the
 438 exact result and the PPA coincide.

Summary 4.3: Limiting cases of kink number distribution

Exact ground-state characteristic function of the kink-number distribution:

$$\tilde{P}_{\beta \rightarrow \infty}(\theta) = \exp(iL\theta/2) \prod_{k \in \mathbf{k}^+} (\cos \theta - i \sin \theta \cos(k - \vartheta_k)). \quad (93)$$

Exact infinite-temperature characteristic function of the kink-number distribution:

$$\tilde{P}_{\beta \rightarrow 0}(\theta) = \exp(iL\theta/2) \left(\cos^L \frac{\theta}{2} + (-1)^{L/2} \sin^L \frac{\theta}{2} \right). \quad (94)$$

439
 440 Instances of the corresponding distributions are shown in Fig. 7 for the (pure) ground-state
 441 as a function the magnetic field. For $g = 0$ one finds a Kronecker delta distribution centered at
 442 $n = 0$, with $P(0) = 1$ and $P(n) = 0$ for $n > 1$, as expected. As the magnetic field is cranked
 443 up, the distribution broadens and gradually shifts away from the origin, becoming approximately
 444 symmetric in the paramagnetic phase.

445 The right panel in Fig. 7 also shows the corresponding distribution in the infinite-temperature
 446 case, that is symmetric, centered at $n = L/2$ and independent of the transverse magnetic field g ,
 447 as can be seen from Eq. (94). In fact, full probability distribution for infinite temperature can
 448 be found by a combinatorial argument. Working in the basis of eigenstates of σ_i^x in each site,
 449 the probability of obtaining $n = 2l$ kinks is related to the number of basis vectors with $2l$ spin

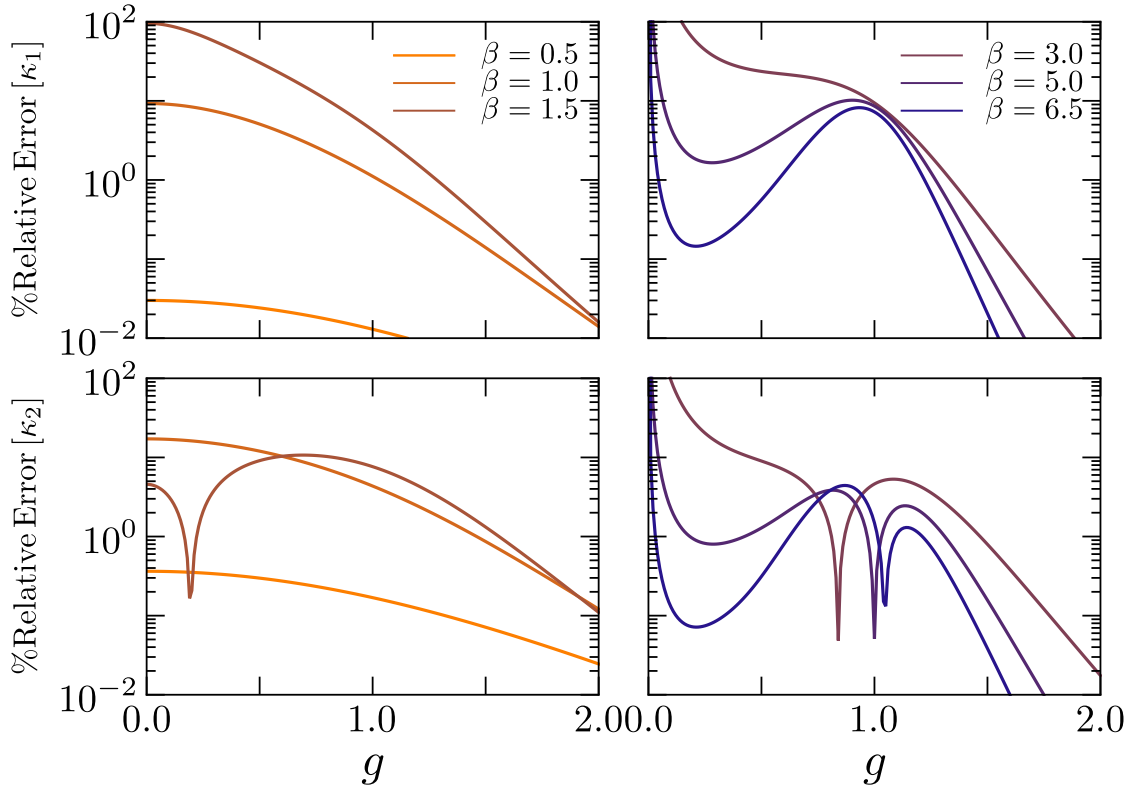


Figure 6: **Relative error for the first two cumulants of the kink-number distribution as a function of magnetic field g .** Using the full characteristic function in Eq. (85) and the PPA characteristic function Eq. (89), the relative error is evaluated as a function of the magnetic field for a system size $L = 12$ and different temperatures.

450 flips, where we use the fact that an even number of kinks is enforced by boundary conditions.
 451 One can choose the location of $2l$ kinks in the chain in $2\binom{L}{2l}$ ways. Therefore, the full probability
 452 distribution has the form:

$$P_{\beta \rightarrow 0}(n = 2l) = \frac{1}{2^{L-1}} \binom{L}{2l}, \quad l = 0, 1, \dots, \frac{L}{2}. \quad (95)$$

453 The corresponding cumulant values read

$$\kappa_1 = \frac{L}{2}, \quad \kappa_2 = \frac{L}{4}, \quad \kappa_3 = 0, \quad \kappa_4 = -\frac{L}{8}, \quad \kappa_5 = 0, \quad \kappa_6 = \frac{L}{4}, \quad \dots \quad (96)$$

454 By keeping the first two cumulants and setting the rest to zero, $P_{\beta \rightarrow 0}(n = 2l)$ can be approximated
 455 by a Gaussian distribution $N(\kappa_1, \kappa_2)$ with mean $\kappa_1 = L/2$ and variance $\kappa_2 = L/4$. As shown in Fig.
 456 7 this approximation describes the envelope of the distribution with great accuracy.

457 **4.2 Probability distribution for the transverse magnetization at thermal equilibrium** 458 **rium**

459 We next focus on the derivation of the explicit form of the characteristic function of the transverse
 460 magnetization

$$\hat{M} = \sum_{n=1}^L \hat{Z}_n, \quad (97)$$

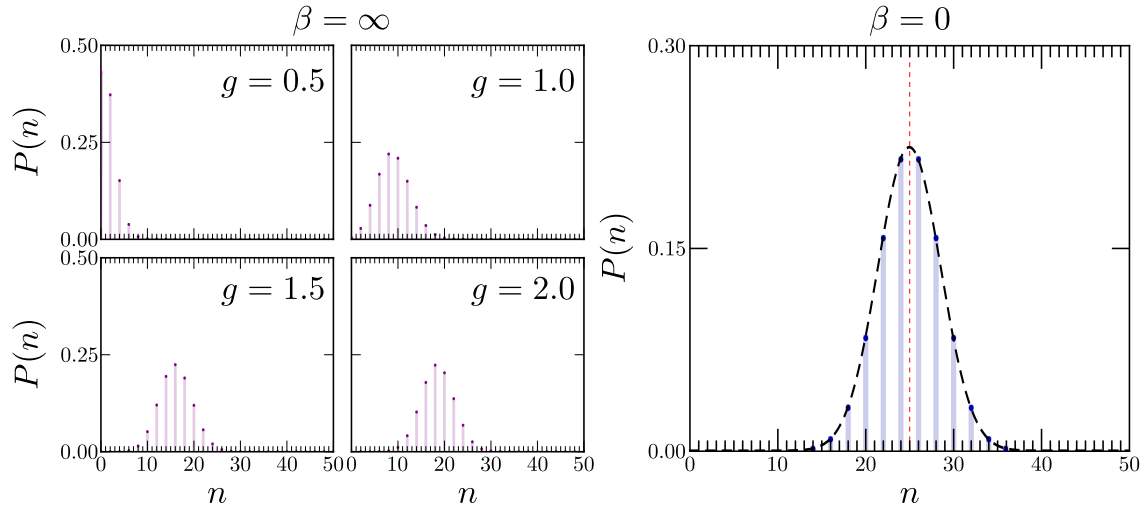


Figure 7: **Limiting cases of kink number distribution.** Probability distribution of the number of kinks $P(n)$ as a function of the magnetic field g and inverse temperature β for a chain of $L = 50$ spins. The left panel shows the kink-number distribution for different values of the magnetic field and is obtained using the ground-state characteristic function Eq. (93). The right panel shows the kink number distribution at infinity temperature, computed using the characterization function given by Eq. (94). The vertical dashed red line is located at $\kappa_1 = L/2$, while the long-dashed black line corresponds to the Gaussian approximation $N(L/2, L/4)$.

461 with eigenvalues $m = -L, -L + 2, \dots, L - 2, L$ for even L . The latter has been studied in the PPA
 462 and continuous approximations and finds broad applications in the characterization of quantum
 463 critical behavior [82–86, 88, 89] and the identification of various many-body states in ultracold-
 464 atom quantum simulators [87].

465 In the Fourier representation, it is the sum of two different contributions:

$$\hat{M}^+ = \sum_{k \in \mathbf{k}^+} 2(\hat{c}_k \hat{c}_k^\dagger - \hat{c}_k^\dagger \hat{c}_k), \quad \hat{M}^- = \sum_{k \in \mathbf{k}^-} 2(\hat{c}_k \hat{c}_k^\dagger - \hat{c}_k^\dagger \hat{c}_k) + \hat{c}_0 \hat{c}_0^\dagger - \hat{c}_0^\dagger \hat{c}_0 + \hat{c}_\pi \hat{c}_\pi^\dagger - \hat{c}_\pi^\dagger \hat{c}_\pi. \quad (98)$$

466 In parallel with Eq. (81), we define a new set of a single-mode operators \hat{m}_k , \hat{m}_0 , and \hat{m}_π ,

$$\hat{m}_k = \begin{pmatrix} 2 & 0 & 0 & 0 \\ 0 & -2 & 0 & 0 \\ 0 & 0 & 0 & 0 \\ 0 & 0 & 0 & 0 \end{pmatrix}, \quad \hat{m}_k^{(1)} = \begin{pmatrix} 2 & 0 \\ 0 & -2 \end{pmatrix}, \quad \hat{m}_k^{(2)} = 0_2. \quad (99)$$

467 In addition, in the negative-parity sector, the matrix \hat{m}_k has the same form for the momenta $0, \pi$
 468 that is given by $\hat{m}_0 = \hat{m}_\pi = \text{diag}(1, -1)$. We can easily compute $\exp(i\theta \hat{m}_k^{(1)})$ and the $\hat{\sigma}_k$ matrix to
 469 obtain

$$\begin{aligned} \hat{\sigma}_k^{(11)} &= \cos(2\theta) + i \cos(\vartheta_k) \sin(2\theta), \\ \hat{\sigma}_k^{(22)} &= \cos(2\theta) - i \cos(\vartheta_k) \sin(2\theta). \end{aligned} \quad (100)$$

Summary 4.4: Full generating function of transverse magnetization

The full characteristic function for the transverse magnetization Eq. (97) at thermal equilibrium reads

$$\tilde{P}(\theta) = \frac{1}{Z(\beta, g, \gamma)} \left(\tilde{P}^+(\theta) + \tilde{P}^-(\theta) \right). \quad (101)$$

Positive part of characteristic function:

$$\begin{aligned} \tilde{P}^+(\theta) = \frac{1}{2} & \left[\prod_{k \in \mathbf{k}^+} 2 (\cos(2\theta) \cosh(\beta \epsilon_k(g, \gamma)) - i \sin(2\theta) \sinh(\beta \epsilon_k(g, \gamma)) \cos(\vartheta_k) + 1) \right. \\ & \left. + \prod_{k \in \mathbf{k}^+} 2 (\cos(2\theta) \cosh(\beta \epsilon_k(g, \gamma)) - i \sin(2\theta) \sinh(\beta \epsilon_k(g, \gamma)) \cos(\vartheta_k) - 1) \right]. \end{aligned} \quad (102)$$

Negative part of characteristic function:

$$\begin{aligned} \tilde{P}^-(\theta) = \frac{1}{2} & \left[\tilde{P}^F(\theta) \prod_{k \in \mathbf{k}^-} 2 (\cos(2\theta) \cosh(\beta \epsilon_k(g, \gamma)) - i \sin(2\theta) \sinh(\beta \epsilon_k(g, \gamma)) \cos(\vartheta_k) + 1) \right. \\ & \left. - \tilde{P}^B(\theta) \prod_{k \in \mathbf{k}^-} 2 (\cos(2\theta) \cosh(\beta \epsilon_k(g, \gamma)) - i \sin(2\theta) \sinh(\beta \epsilon_k(g, \gamma)) \cos(\vartheta_k) - 1) \right], \end{aligned} \quad (103)$$

with

$$\begin{aligned} \tilde{P}^F(\theta) &= 2^2 \cosh\left(\frac{\beta \epsilon_{k=0} + 2i\theta}{2}\right) \cosh\left(\frac{\beta \epsilon_{k=\pi} + 2i\theta}{2}\right), \\ \tilde{P}^B(\theta) &= 2^2 \sinh\left(\frac{\beta \epsilon_{k=0} + 2i\theta}{2}\right) \sinh\left(\frac{\beta \epsilon_{k=\pi} + 2i\theta}{2}\right). \end{aligned} \quad (104)$$

The exact partition function is given by Eq. (48), with the eigenenergies $\epsilon_k(g, \gamma)$ and $\epsilon_{k=0}$ given by Eq. (47), and the Bogoliubov angles ϑ_k satisfying Eq. (17).

470

By contrast, in the PPA, the characteristic function of the transverse magnetization in the thermodynamic limit contains only the first term of $\tilde{P}^+(\theta)$:

471

472

473

474

Summary 4.5: PPA characteristic function for transverse magnetization

In the thermodynamic limit, Eq. (101) reduces to

$$\tilde{P}_{\text{PPA}}(\theta) = \frac{1}{2Z_F^+(\beta, g, \gamma)} \prod_{k \in \mathbf{k}^+} 2 (\cos(2\theta) \cosh(\beta \epsilon_k(g, \gamma)) - i \sin(2\theta) \sinh(\beta \epsilon_k(g, \gamma)) \cos(\vartheta_k) + 1), \quad (105)$$

where $Z_F^+(\beta, g, \gamma)$ is defined in (49).

475

The magnetization distribution is shown in Fig. 8 for different values of g and β for a fixed system size $L = 50$. The distribution $P(m)$ vanishes for odd values of m for even L . It is naturally symmetric for $g = 0$ and approximately so for finite g in the high-temperature case at low magnetic fields, when it approaches a binomial distribution. The accuracy of the PPA is remarkable as a function of g and β with discrepancies being noticeable in the pure ferromagnet ($g = 0$) at low temperature. As the magnetic field is cranked up at constant β , the alignment of the spins is favored shifting the mean and increasing the negative skewness of the distribution in the paramagnetic phase.

476

477

478

479

480

481

482

483

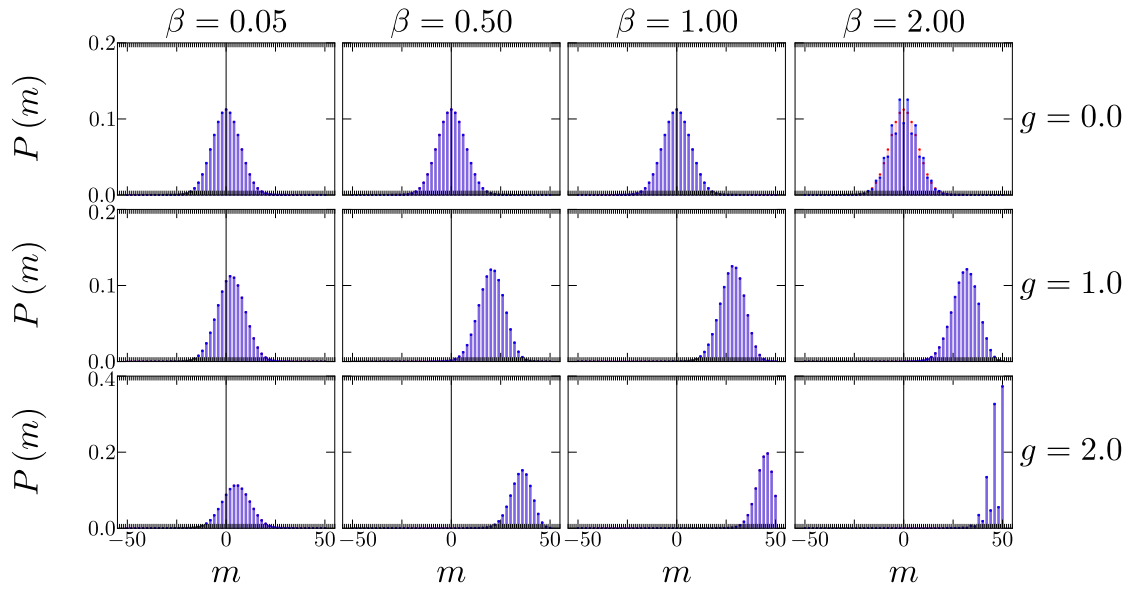


Figure 8: **Magnetization distribution at thermodynamic equilibrium.** Probability distribution of the transverse magnetization $P(m)$ for different values of the magnetic field g and inverse temperature β in a chain of $L = 50$ spins. The exact probability distribution Eq. (101) (red bars) is compared with the simplified expression in Eq. (105) (blue bars).

484 Figure 9 provides a systematic characterization of the first two cumulants as a function of
 485 the inverse temperature for different values of g . In contrast with the kink-number distribution,
 486 in the ferromagnetic phase the variance always exceeds the mean, and thus the magnetization
 487 distribution remains super-Poissonian. In the paramagnetic phase, at any fixed value of g the
 488 variance decreases with temperature, while the converse is true for the mean magnetization. As a
 489 result, the character of the distribution changes from super-Poissonian to sub-Poissonian as the
 490 temperature is lowered. The behavior of $P(m)$ is shown to be robust as a function of the system
 491 size, with discrepancies between the exact results and the PPA being restricted to the critical point.
 492 The relative error of the PPA remains below 10% as a function of g and β as shown in Fig. 10.

493 As in the case of kink number distribution, we close with a characterization of the magnetiza-
 494 tion distribution in the limits of infinite and vanishing inverse temperature β .

Summary 4.6: Limiting cases of transverse magnetization distribution

Exact ground-state characteristic function of transverse magnetization:

$$\tilde{P}_{\beta \rightarrow \infty}(\theta) = \prod_{k \in \mathbf{k}^+} (\cos 2\theta - i \sin 2\theta \cos \vartheta_k). \quad (106)$$

Exact infinite-temperature characteristic function of transverse magnetization:

$$\tilde{P}_{\beta \rightarrow 0}(\theta) = \cos^L \theta. \quad (107)$$

495

496 The behavior of the ground-state magnetization distribution is the reverse of the kink-number
 497 distribution in the sense that it becomes approximately symmetric in the ferromagnetic phase and
 498 sharply peaked at $m = L$ in the paramagnetic phase. Using formulas (106) and (63), one can find
 499 the first cumulants of the ground-state distribution explicitly. In particular, the first few cumulants

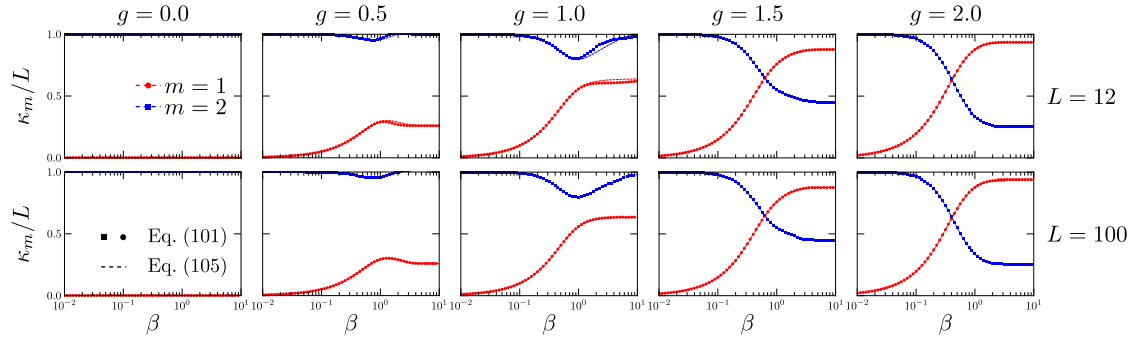


Figure 9: **Cumulants of the magnetization distribution as a function of the inverse of temperature β .** Using the full characteristic function given by Eq. (101), the mean value of the transversal magnetization κ_1 and the variance κ_2 are shown by red circles and blue squares, respectively. The dashed lines correspond to the numerical results using the simplified characteristic function (Eq. (105)). In the ferromagnetic phase the statistics is super-Poissonian, while it changes from super- to sub-Poissonian in the paramagnetic phase as the temperature is decreased. The magnetic field varies from 0.0 to 2.0 from left to right in steps of 0.5. The system size is $L = 12$ in the upper row and $L = 100$ in the lower one.

500 read

$$\kappa_1 = - \sum_{k \in \mathbf{k}^+} 2 \cos \vartheta_k, \quad (108)$$

$$\kappa_2 = L - 2 \sum_{k \in \mathbf{k}^+} \cos(2\vartheta_k), \quad (109)$$

$$\kappa_3 = 4 \sum_{k \in \mathbf{k}^+} [\cos(\vartheta_k) - \cos(3\vartheta_k)]. \quad (110)$$

501 The second cumulant turns out to have a particularly simple form due to its close relation to the
 502 ground-state fidelity susceptibility [74, 94] and reads

$$\kappa_2 = L \frac{1 + g^{L-2}}{1 + g^L}. \quad (111)$$

503

504 By contrast, in the infinite-temperature case, in which the PPA is exact, the distribution is sym-
 505 metric, centered at $m = 0$ and independent of the magnetic field. The magnetization distribution
 506 describes in this case the sum of L independent discrete random variables with outcomes ± 1 with
 507 equal probability $1/2$. As a result $\kappa_1 = 0$, $\kappa_2 = L/4$. In the infinite temperature limit, $P(m)$ is equal
 508 to that of a classical Ising chain and can be written explicitly:

$$P_{\beta \rightarrow 0}(m) = \frac{1}{2^L} \binom{L}{\frac{1}{2}(m+L)}, \quad m = -L, -L+2, \dots, L-2, L. \quad (112)$$

509 Odd cumulant identically vanish, while the first even ones read

$$\kappa_2 = L, \quad \kappa_4 = -2L, \quad \kappa_6 = 16L, \quad \kappa_8 = -272L, \quad \kappa_{10} = 7936L, \quad \dots \quad (113)$$

510 As a result, in the normal approximation $P_{\beta \rightarrow 0}(n = 2l)$ is given by Gaussian distribution with
 511 zero mean and variance $\kappa_2 = L$. Fig. 11 shows this Gaussian distribution as a black envelope,
 512 accurately approximating the exact results.

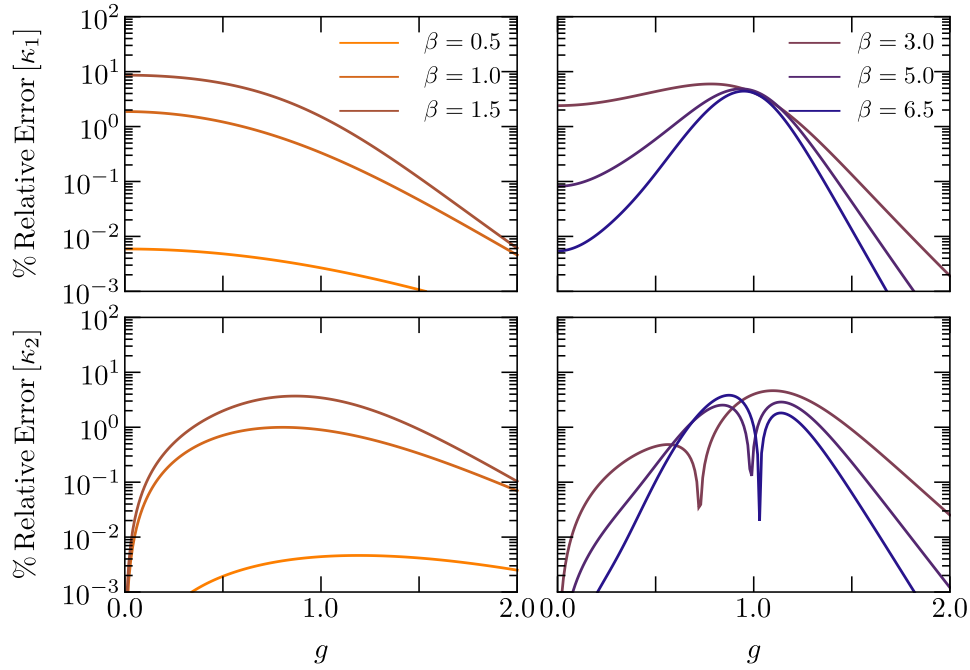


Figure 10: **Relative error for the first two cumulants of the magnetization distribution as a function of magnetic field g .** Using the full characteristic function in Eq. (101) and the corresponding PPA Eq. (105), the relative error is evaluated as a function of the magnetic field for a system size $L = 12$ and different temperatures.

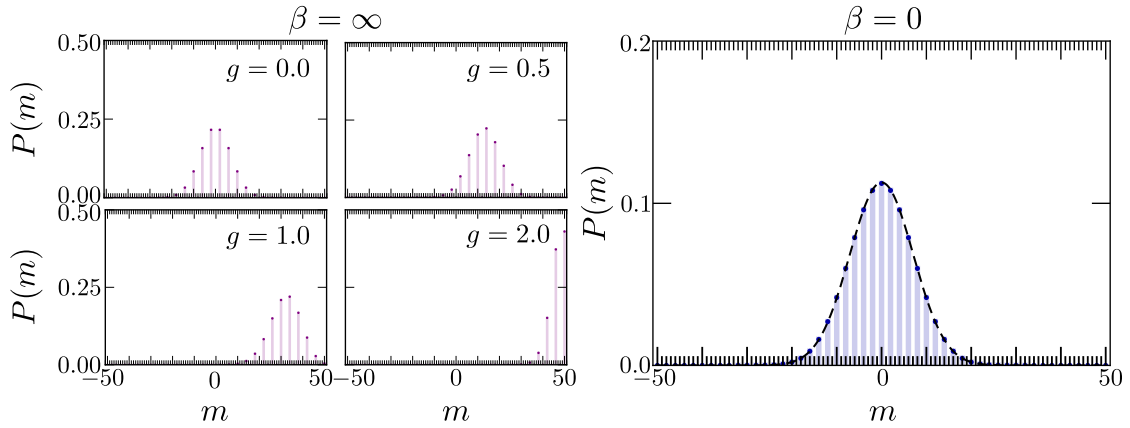


Figure 11: **Limiting cases of transverse magnetization distribution.** Probability distribution of the transverse magnetization $P(m)$ as a function of the magnetic field g and inverse temperature β for a chain of $L = 50$ spins. The left panel shows the ground-state transverse magnetization distribution for different values of the magnetic field, and is computed using the characteristic function Eq. (106). The right panel shows the transverse magnetization distribution at infinity temperature, obtained using the characterization function given by Eq. (107). The envelope of the distribution is reproduced by the Gaussian approximation $N(0, L)$ shown as a dashed black line.

513 **5 Conclusion**

514 We have provided an exact treatment of the thermal equilibrium properties for a class of integrable
515 spin chains that admit a description in terms of free fermions. Instances of this family are the
516 one-dimensional transverse-field Ising, XY and Kitaev models, among other examples. Whenever
517 the system Hamiltonian commutes with parity operator, the complete Hilbert spaces is the direct
518 sum of the corresponding even and odd parity subspaces. For an exact treatment of thermal equi-
519 librium, we have detailed an algebraic approach in the complete Hilbert spaces and provided the
520 exact expression for the partition function. We have identified the limitations of the approximate
521 description of thermal equilibrium in terms of the positive-parity sector, frequently adopted in the
522 literature. This approximate approach fails in what can be considered the most interesting regime:
523 the neighborhood of a quantum critical point at low temperatures. In particular, we have shown
524 that the discrepancies between the exact and approximate results can lead to significant errors in
525 this regime.

526 Making use of the exact algebraic framework, we have computed as well the eigenvalue prob-
527 ability distribution of different observables. As an application, we have characterized in detail the
528 distribution of the number of kinks as well as the transverse magnetization, covering all regimes
529 from zero temperature (ground-state behavior) to infinite temperature. Our results are of direct
530 relevance to the study of thermal equilibrium properties of integrable spin chains as well as the
531 study of the nonequilibrium dynamics generated by driving a thermal state out of equilibrium.
532 They are thus expected to find applications in the description of quantum simulation experiments,
533 quantum annealing and quantum thermodynamics of spin systems. As a prospect, it is interesting
534 to extend our results to the generalized Gibbs state whenever the relaxing dynamics of an initial
535 state preserves a set of integrals of motion.

536 **Acknowledgements**

537 We thank Bogdan Damski, Jacek Dziarmaga and Victor Mukherjee for insightful remarks con-
538 cerning the manuscript.

539 **Funding information** We acknowledge funding support from the Spanish Ministerio de Ciencia
540 e Innovación (PID2019-109007GA-I00). MB acknowledges support of Polish National Science
541 Center (NCN) grant DEC-2016/23/B/ST3/01152 and Faculty of Physics, astronomy and Computer
542 Science internal grant N17/MNS/000008.

543 A Proof Proposition 2: Identities for Traces

544 First, the formulas given by Eq. (34) are true for $n = 1$. We assume that they are true for some
545 $n \geq 1$ and we compute

$$\begin{aligned} \operatorname{tr} \left[\mathcal{P} \left(\bigotimes_{i=1}^{n+1} \hat{O}_{k_i} \right) \right] &= \operatorname{tr} \left[\mathcal{P} \left(\bigotimes_{i=1}^n \hat{O}_{k_i} \right) \right] \cdot \operatorname{tr} \left[\hat{O}_{k_{n+1}}^{(p)} \right] + \operatorname{tr} \left[\mathcal{N} \left(\bigotimes_{i=1}^n O_{k_i} \right) \right] \cdot \operatorname{tr} \left[\hat{O}_{k_{n+1}}^{(n)} \right] \\ &= \frac{1}{2} \left[\left(\operatorname{tr} \left[\hat{O}_{k_{n+1}}^{(p)} \right] + \operatorname{tr} \left[\hat{O}_{k_{n+1}}^{(n)} \right] \right) \prod_{i=1}^n \operatorname{tr} \left[\hat{O}_{k_i} \right] \right. \\ &\quad \left. + \left(\operatorname{tr} \left[\hat{O}_{k_{n+1}}^{(p)} \right] - \operatorname{tr} \left[\hat{O}_{k_{n+1}}^{(n)} \right] \right) \prod_{i=1}^n \left(\operatorname{tr} \left[\hat{O}_{k_i}^{(p)} \right] - \operatorname{tr} \left[\hat{O}_{k_i}^{(n)} \right] \right) \right] \\ &= \frac{1}{2} \left[\prod_{i=1}^{n+1} \operatorname{tr} \left[\hat{O}_{k_i} \right] + \prod_{i=1}^{n+1} \left(\operatorname{tr} \left[\hat{O}_{k_i}^{(p)} \right] - \operatorname{tr} \left[\hat{O}_{k_i}^{(n)} \right] \right) \right], \end{aligned}$$

546 and an inductive step is completed.

547 References

- 548 [1] S. Sachdev, *Quantum Phase Transitions, Second Edition*, Cambridge University Press,
549 Cambridge (2011).
- 550 [2] B. K. Chakrabarti, A. Dutta and P. Sen, *Quantum Ising Phases and Transitions in Transverse
551 Ising Models*, vol. m41, Springer-Verlag, Berlin (1996).
- 552 [3] S. Suzuki, J. ichi Inoue and B. K. Chakrabarti, *Quantum Ising Phases and Transitions in
553 Transverse Ising Models*, Springer, 2 edn., doi:10.1007/978-3-642-33039-1 (2013).
- 554 [4] A. Dutta, G. Aeppli, B. K. Chakrabarti, U. Divakaran, T. F. Rosenbaum and D. Sen, *Quantum
555 Phase Transitions in Transverse Field Spin Models: From Statistical Physics to Quantum
556 Information*, Cambridge University Press, doi:10.1017/CBO9781107706057 (2015).
- 557 [5] E. Lieb, T. Schultz and D. Mattis, *Two soluble models of an antiferromagnetic chain*, *Annals of
558 Physics* **16**(3), 407 (1961), doi:https://doi.org/10.1016/0003-4916(61)90115-4.
- 559 [6] P. Pfeuty, *The one-dimensional ising model with a transverse field*, *Annals of Physics* **57**(1),
560 79 (1970), doi:https://doi.org/10.1016/0003-4916(70)90270-8.
- 561 [7] A. Kitaev, *Anyons in an exactly solved model and beyond*, *Annals of Physics* **321**(1), 2
562 (2006), doi:https://doi.org/10.1016/j.aop.2005.10.005, January Special Issue.
- 563 [8] S. Sachdev, *Universal, finite-temperature, crossover functions of the quantum transi-
564 tion in the Ising chain in a transverse field*, *Nuclear Physics B* **464**(3), 576 (1996),
565 doi:https://doi.org/10.1016/0550-3213(95)00657-5.
- 566 [9] A. Leclair, F. Lesage, S. Sachdev and H. Saleur, *Finite temperature correlations in
567 the one-dimensional quantum Ising model*, *Nuclear Physics B* **482**(3), 579 (1996),
568 doi:https://doi.org/10.1016/S0550-3213(96)00456-7.
- 569 [10] S. Sachdev and A. P. Young, *Low temperature relaxational dynamics of the Ising chain in a
570 transverse field*, *Phys. Rev. Lett.* **78**, 2220 (1997), doi:10.1103/PhysRevLett.78.2220.

- 571 [11] A. Polkovnikov, *Universal adiabatic dynamics in the vicinity of a quantum critical point*,
572 Phys. Rev. B **72**, 161201 (2005), doi:10.1103/PhysRevB.72.161201.
- 573 [12] J. Dziarmaga, *Dynamics of a quantum phase transition: Exact solution of the quantum Ising*
574 *model*, Phys. Rev. Lett. **95**, 245701 (2005), doi:10.1103/PhysRevLett.95.245701.
- 575 [13] M. Gong, X. Wen, G. Sun, D.-W. Zhang, D. Lan, Y. Zhou, Y. Fan, Y. Liu, X. Tan, H. Yu,
576 Y. Yu, S.-L. Zhu *et al.*, *Simulating the Kibble-Zurek mechanism of the Ising model with a su-*
577 *perconducting qubit system*, Scientific Reports **6**(1), 22667 (2016), doi:10.1038/srep22667.
- 578 [14] J.-M. Cui, Y.-F. Huang, Z. Wang, D.-Y. Cao, J. Wang, W.-M. Lv, L. Luo, A. del Campo, Y.-J.
579 Han, C.-F. Li and G.-C. Guo, *Experimental trapped-ion quantum simulation of the Kibble-*
580 *Zurek dynamics in momentum space*, Sci. Rep. **6**, 33381 (2016), doi:10.1038/srep33381.
- 581 [15] A. Keesling, A. Omran, H. Levine, H. Bernien, H. Pichler, S. Choi, R. Samajdar, S. Schwartz,
582 P. Silvi, S. Sachdev, P. Zoller, M. Endres *et al.*, *Quantum Kibble-Zurek mechanism and*
583 *critical dynamics on a programmable Rydberg simulator*, Nature **568**(7751), 207 (2019),
584 doi:10.1038/s41586-019-1070-1.
- 585 [16] Y. Bando, Y. Susa, H. Oshiyama, N. Shibata, M. Ohzeki, F. J. Gómez-Ruiz, D. A. Lidar,
586 S. Suzuki, A. del Campo and H. Nishimori, *Probing the universality of topological defect*
587 *formation in a quantum annealer: Kibble-Zurek mechanism and beyond*, Phys. Rev. Re-
588 search **2**, 033369 (2020), doi:10.1103/PhysRevResearch.2.033369.
- 589 [17] D. Sen, K. Sengupta and S. Mondal, *Defect production in nonlinear quench*
590 *across a quantum critical point*, Phys. Rev. Lett. **101**, 016806 (2008),
591 doi:10.1103/PhysRevLett.101.016806.
- 592 [18] R. Barankov and A. Polkovnikov, *Optimal nonlinear passage through a quantum critical*
593 *point*, Phys. Rev. Lett. **101**, 076801 (2008), doi:10.1103/PhysRevLett.101.076801.
- 594 [19] A. del Campo, T. W. B. Kibble and W. H. Zurek, *Causality and non-equilibrium second-*
595 *order phase transitions in inhomogeneous systems*, J. Phys. Cond. Mat. **25**(40), 404210
596 (2013), doi:10.1088/0953-8984/25/40/404210.
- 597 [20] J. Dziarmaga and M. M. Rams, *Dynamics of an inhomogeneous quantum phase transition*,
598 New J. Phys. **12**(5), 055007 (2010), doi:10.1088/1367-2630/12/5/055007.
- 599 [21] J. Dziarmaga and M. M. Rams, *Adiabatic dynamics of an inhomogeneous quantum phase*
600 *transition: the case of a $z > 1$ dynamical exponent*, New J. Phys. **12**(10), 103002 (2010),
601 doi:10.1088/1367-2630/12/10/103002.
- 602 [22] M. M. Rams, M. Mohseni and A. del Campo, *Inhomogeneous quasi-adiabatic driving of*
603 *quantum critical dynamics in weakly disordered spin chains*, New J. Phys. **18**, 123034
604 (2016), doi:10.1088/1367-2630/aa5079.
- 605 [23] F. J. Gómez-Ruiz and A. del Campo, *Universal dynamics of inhomogeneous quantum*
606 *phase transitions: Suppressing defect formation*, Phys. Rev. Lett. **122**, 080604 (2019),
607 doi:10.1103/PhysRevLett.122.080604.
- 608 [24] D. Patanè, A. Silva, L. Amico, R. Fazio and G. E. Santoro, *Adiabatic dynamics*
609 *in open quantum critical many-body systems*, Phys. Rev. Lett. **101**, 175701 (2008),
610 doi:10.1103/PhysRevLett.101.175701.

- 611 [25] A. Dutta, A. Rahmani and A. del Campo, *Anti-Kibble-Zurek behavior in crossing the quan-*
612 *tum critical point of a thermally isolated system driven by a noisy control field*, Phys. Rev.
613 Lett. **117**, 080402 (2016), doi:10.1103/PhysRevLett.117.080402.
- 614 [26] M.-Z. Ai, J.-M. Cui, R. He, Z.-H. Qian, X.-X. Gao, Y.-F. Huang, C.-F. Li and G.-C. Guo,
615 *Experimental verification of anti-Kibble-Zurek behavior in a quantum system under a noisy*
616 *control field*, Phys. Rev. A **103**, 012608 (2021), doi:10.1103/PhysRevA.103.012608.
- 617 [27] L. Cincio, J. Dziarmaga, M. M. Rams and W. H. Zurek, *Entropy of entanglement and corre-*
618 *lations induced by a quench: Dynamics of a quantum phase transition in the quantum Ising*
619 *model*, Phys. Rev. A **75**, 052321 (2007), doi:10.1103/PhysRevA.75.052321.
- 620 [28] A. del Campo, *Universal statistics of topological defects formed in a quantum phase transi-*
621 *tion*, Phys. Rev. Lett. **121**, 200601 (2018), doi:10.1103/PhysRevLett.121.200601.
- 622 [29] J.-M. Cui, F. J. Gómez-Ruiz, Y.-F. Huang, C.-F. Li, G.-C. Guo and A. del Campo, *Exper-*
623 *imentally testing quantum critical dynamics beyond the Kibble-Zurek mechanism*, Comm.
624 Phys. **3**, 44 (2020), doi:10.1038/s42005-020-0306-6.
- 625 [30] F. J. Gómez-Ruiz, J. J. Mayo and A. del Campo, *Full counting statistics of topolog-*
626 *ical defects after crossing a phase transition*, Phys. Rev. Lett. **124**, 240602 (2020),
627 doi:10.1103/PhysRevLett.124.240602.
- 628 [31] A. del Campo, F. J. Gómez-Ruiz, Z.-H. Li, C.-Y. Xia, H.-B. Zeng and H.-Q. Zhang, *Univer-*
629 *sal statistics of vortices in a newborn holographic superconductor: Beyond the Kibble-Zurek*
630 *mechanism* (2021), 2101.02171.
- 631 [32] A. del Campo, M. M. Rams and W. H. Zurek, *Assisted finite-rate adiabatic passage across*
632 *a quantum critical point: Exact solution for the quantum Ising model*, Phys. Rev. Lett. **109**,
633 115703 (2012), doi:10.1103/PhysRevLett.109.115703.
- 634 [33] K. Takahashi, *Transitionless quantum driving for spin systems*, Phys. Rev. E **87**, 062117
635 (2013), doi:10.1103/PhysRevE.87.062117.
- 636 [34] H. Saberi, T. Opatrny, K. Mølmer and A. del Campo, *Adiabatic tracking of quantum many-*
637 *body dynamics*, Phys. Rev. A **90**, 060301 (2014), doi:10.1103/PhysRevA.90.060301.
- 638 [35] J. D. Sau and K. Sengupta, *Suppressing defect production during passage through a quantum*
639 *critical point*, Phys. Rev. B **90**, 104306 (2014), doi:10.1103/PhysRevB.90.104306.
- 640 [36] N. Wu, A. Nanduri and H. Rabitz, *Optimal suppression of defect generation dur-*
641 *ing a passage across a quantum critical point*, Phys. Rev. B **91**, 041115 (2015),
642 doi:10.1103/PhysRevB.91.041115.
- 643 [37] A. del Campo and K. Sengupta, *Controlling quantum critical dynamics of isolated systems*,
644 Euro. Phys. J. Spe. Top. **224**(1), 189 (2015).
- 645 [38] P. W. Claeys, M. Pandey, D. Sels and A. Polkovnikov, *Floquet-engineering counterdia-*
646 *batic protocols in quantum many-body systems*, Phys. Rev. Lett. **123**, 090602 (2019),
647 doi:10.1103/PhysRevLett.123.090602.
- 648 [39] M. M. Rams, J. Dziarmaga and W. H. Zurek, *Symmetry breaking bias and the*
649 *dynamics of a quantum phase transition*, Phys. Rev. Lett. **123**, 130603 (2019),
650 doi:10.1103/PhysRevLett.123.130603.

- 651 [40] G. Passarelli, V. Cataudella, R. Fazio and P. Lucignano, *Counterdiabatic driving in the*
652 *quantum annealing of the p -spin model: A variational approach*, Phys. Rev. Research **2**,
653 013283 (2020), doi:10.1103/PhysRevResearch.2.013283.
- 654 [41] K. Suzuki and K. Takahashi, *Performance evaluation of adiabatic quantum computation via*
655 *quantum speed limits and possible applications to many-body systems*, Phys. Rev. Research
656 **2**, 032016 (2020), doi:10.1103/PhysRevResearch.2.032016.
- 657 [42] L. Prielinger, A. Hartmann, Y. Yamashiro, K. Nishimura, W. Lechner and H. Nishimori,
658 *Diabatic quantum annealing by counter-diabatic driving* (2020), 2011.02691.
- 659 [43] A. Silva, *Statistics of the work done on a quantum critical system by quenching a control*
660 *parameter*, Phys. Rev. Lett. **101**, 120603 (2008), doi:10.1103/PhysRevLett.101.120603.
- 661 [44] R. Dorner, J. Goold, C. Cormick, M. Paternostro and V. Vedral, *Emergent thermody-*
662 *namics in a quenched quantum many-body system*, Phys. Rev. Lett. **109**, 160601 (2012),
663 doi:10.1103/PhysRevLett.109.160601.
- 664 [45] Z. Fei and H. T. Quan, *Group-theoretical approach to the calculation of quantum work dis-*
665 *tribution*, Phys. Rev. Research **1**, 033175 (2019), doi:10.1103/PhysRevResearch.1.033175.
- 666 [46] Z. Fei, N. Freitas, V. Cavina, H. T. Quan and M. Esposito, *Work statis-*
667 *tics across a quantum phase transition*, Phys. Rev. Lett. **124**, 170603 (2020),
668 doi:10.1103/PhysRevLett.124.170603.
- 669 [47] R. B. S. V. Mukherjee, U. Divakaran and A. del Campo, *Universal finite-time thermody-*
670 *namics of many-body quantum machines from Kibble-Zurek scaling*, Phys. Rev. Research **2**,
671 043247 (2020), doi:10.1103/PhysRevResearch.2.043247.
- 672 [48] R. Coldea, D. A. Tennant, E. M. Wheeler, E. Wawrzynska, D. Prabhakaran, M. Telling,
673 K. Habicht, P. Smeibidl and K. Kiefer, *Quantum criticality in an Ising chain: Ex-*
674 *perimental evidence for emergent E_8 symmetry*, Science **327**(5962), 177 (2010),
675 doi:10.1126/science.1180085.
- 676 [49] D. Porras and J. I. Cirac, *Effective quantum spin systems with trapped ions*, Phys. Rev. Lett.
677 **92**, 207901 (2004), doi:10.1103/PhysRevLett.92.207901.
- 678 [50] A. Friedenauer, H. Schmitz, J. T. Glueckert, D. Porras and T. Schaetz, *Simulating a quantum*
679 *magnet with trapped ions*, Nature Physics **4**(10), 757 (2008), doi:10.1038/nphys1032.
- 680 [51] K. Kim, M.-S. Chang, S. Korenblit, R. Islam, E. E. Edwards, J. K. Freericks, G.-D. Lin,
681 L.-M. Duan and C. Monroe, *Quantum simulation of frustrated Ising spins with trapped ions*,
682 Nature **465**(7298), 590 (2010), doi:10.1038/nature09071.
- 683 [52] R. Islam, E. E. Edwards, K. Kim, S. Korenblit, C. Noh, H. Carmichael, G.-D. Lin, L.-M.
684 Duan, C.-C. Joseph Wang, J. K. Freericks and C. Monroe, *Onset of a quantum phase tran-*
685 *sition with a trapped ion quantum simulator*, Nature Communications **2**(1), 377 (2011),
686 doi:10.1038/ncomms1374.
- 687 [53] P. Richerme, Z.-X. Gong, A. Lee, C. Senko, J. Smith, M. Foss-Feig, S. Michalakis, A. V.
688 Gorshkov and C. Monroe, *Non-local propagation of correlations in quantum systems with*
689 *long-range interactions*, Nature **511**(7508), 198 (2014), doi:10.1038/nature13450.
- 690 [54] J. Simon, W. S. Bakr, R. Ma, M. E. Tai, P. M. Preiss and M. Greiner, *Quantum simula-*
691 *tion of antiferromagnetic spin chains in an optical lattice*, Nature **472**(7343), 307 (2011),
692 doi:10.1038/nature09994.

- 693 [55] M. W. Johnson, M. H. S. Amin, S. Gildert, T. Lanting, F. Hamze, N. Dickson, R. Harris, A. J.
694 Berkley, J. Johansson, P. Bunyk, E. M. Chapple, C. Enderud *et al.*, *Quantum annealing with*
695 *manufactured spins*, Nature **473**(7346), 194 (2011), doi:10.1038/nature10012.
- 696 [56] Y. Salathé, M. Mondal, M. Oppliger, J. Heinsoo, P. Kurpiers, A. Potočnik, A. Mezzacapo,
697 U. Las Heras, L. Lamata, E. Solano, S. Filipp and A. Wallraff, *Digital quantum simula-*
698 *tion of spin models with circuit quantum electrodynamics*, Phys. Rev. X **5**, 021027 (2015),
699 doi:10.1103/PhysRevX.5.021027.
- 700 [57] R. Barends, A. Shabani, L. Lamata, J. Kelly, A. Mezzacapo, U. L. Heras, R. Bab-
701 bush, A. G. Fowler, B. Campbell, Y. Chen, Z. Chen, B. Chiaro *et al.*, *Digitized adia-*
702 *batic quantum computing with a superconducting circuit*, Nature **534**(7606), 222 (2016),
703 doi:10.1038/nature17658.
- 704 [58] A. Cervera-Lierta, *Exact Ising model simulation on a quantum computer*, Quantum **2**, 114
705 (2018), doi:10.22331/q-2018-12-21-114.
- 706 [59] H. T. Quan and F. M. Cucchietti, *Quantum fidelity and thermal phase transitions*, Phys. Rev.
707 E **79**, 031101 (2009), doi:10.1103/PhysRevE.79.031101.
- 708 [60] X.-M. Lu, Z. Sun, X. Wang and P. Zanardi, *Operator fidelity susceptibility, decoherence, and*
709 *quantum criticality*, Phys. Rev. A **78**, 032309 (2008), doi:10.1103/PhysRevA.78.032309.
- 710 [61] A. Lamacraft and P. Fendley, *Order parameter statistics in the critical quantum Ising chain*,
711 Phys. Rev. Lett. **100**, 165706 (2008), doi:10.1103/PhysRevLett.100.165706.
- 712 [62] S. Deng, G. Ortiz and L. Viola, *Dynamical critical scaling and effective thermaliza-*
713 *tion in quantum quenches: Role of the initial state*, Phys. Rev. B **83**, 094304 (2011),
714 doi:10.1103/PhysRevB.83.094304.
- 715 [63] S. Katsura, *Statistical mechanics of the anisotropic linear Heisenberg model*, Phys. Rev.
716 **127**, 1508 (1962), doi:10.1103/PhysRev.127.1508.
- 717 [64] E. Barouch and B. M. McCoy, *Statistical mechanics of the XY model. II. spin-correlation*
718 *functions*, Phys. Rev. A **3**, 786 (1971), doi:10.1103/PhysRevA.3.786.
- 719 [65] V. S. Kapitonov and K. N. Il'inskii, *Functional representations for correlators of spin chains*,
720 Journal of Mathematical Sciences **88**(2), 233 (1998), doi:10.1007/BF02364984.
- 721 [66] J. Zhang, G. Pagano, P. W. Hess, A. Kyprianidis, P. Becker, H. Kaplan, A. V. Gorshkov,
722 Z.-X. Gong and C. Monroe, *Observation of a many-body dynamical phase transition with a*
723 *53-qubit quantum simulator*, Nature **551**, 601 (2017), doi:10.1038/nature24654.
- 724 [67] A. Keesling, A. Omran, H. Levine, H. Bernien, H. Pichler, S. Choi, R. Samajdar, S. Schwartz,
725 P. Silvi, S. Sachdev, P. Zoller, M. Endres *et al.*, *Quantum Kibble-Zurek mechanism and*
726 *critical dynamics on a programmable Rydberg simulator*, Nature **568**(7751), 207 (2019),
727 doi:10.1038/s41586-019-1070-1.
- 728 [68] P. Jordan and E. Wigner, *Über das paulische äquivalenzverbot*, Zeitschrift für Physik **47**(9),
729 631 (1928), doi:10.1007/BF01331938.
- 730 [69] E. Barouch, B. M. McCoy and M. Dresden, *Statistical mechanics of the XY model. I*, Phys.
731 Rev. A **2**, 1075 (1970), doi:10.1103/PhysRevA.2.1075.
- 732 [70] E. Barouch and B. M. McCoy, *Statistical mechanics of the XY model. III*, Phys. Rev. A **3**,
733 2137 (1971), doi:10.1103/PhysRevA.3.2137.

- 734 [71] B. M. McCoy, E. Barouch and D. B. Abraham, *Statistical mechanics of the XY*
735 *model. IV. time-dependent spin-correlation functions*, Phys. Rev. A **4**, 2331 (1971),
736 doi:10.1103/PhysRevA.4.2331.
- 737 [72] C. Itzykson and J.-M. Drouffe, *Statistical Field Theory*, vol. 1 of *Cambridge Monographs*
738 *on Mathematical Physics*, Cambridge University Press, doi:10.1017/CBO9780511622779
739 (1989).
- 740 [73] M. Takahashi, *Thermodynamics of One-Dimensional Solvable Models*, Cambridge Univer-
741 sity Press, doi:10.1017/CBO9780511524332 (1999).
- 742 [74] B. Damski and M. M. Rams, *Exact results for fidelity susceptibility of the quantum Ising*
743 *model: the interplay between parity, system size, and magnetic field*, Journal of Physics A:
744 Mathematical and Theoretical **47**(2), 025303 (2013), doi:10.1088/1751-8113/47/2/025303.
- 745 [75] M. Okuyama, Y. Yamanaka, H. Nishimori and M. M. Rams, *Anomalous behavior of the*
746 *energy gap in the one-dimensional quantum XY model*, Phys. Rev. E **92**, 052116 (2015),
747 doi:10.1103/PhysRevE.92.052116.
- 748 [76] Z. Xu and A. del Campo, *Probing the full distribution of many-body ob-*
749 *servables by single-qubit interferometry*, Phys. Rev. Lett. **122**, 160602 (2019),
750 doi:10.1103/PhysRevLett.122.160602.
- 751 [77] L. S. Levitov and G. B. Lesovik, *Charge distribution in quantum shot noise*, JETP Lett. **58**,
752 230 (1993).
- 753 [78] L. S. Levitov, H. Lee and G. B. Lesovik, *Electron counting statistics and coher-*
754 *ent states of electric current*, Journal of Mathematical Physics **37**(10), 4845 (1996),
755 doi:10.1063/1.531672.
- 756 [79] I. Klich, *An Elementary Derivation of Levitov's Formula*, pp. 397–402, Springer Nether-
757 lands, Dordrecht, ISBN 978-94-010-0089-5, doi:10.1007/978-94-010-0089-5_19 (2003).
- 758 [80] F. Haake, *Quantum Signatures of Chaos*, Springer, Berlin (2010).
- 759 [81] F. Binder, L. Correa, C. Gogolin, J. Anders and G. Adesso, *Thermodynamics in the Quan-*
760 *tum Regime: Fundamental Aspects and New Directions*, Fundamental Theories of Physics.
761 Springer International Publishing, ISBN 9783319990460 (2019).
- 762 [82] K. Binder, *Finite size scaling analysis of Ising model block distribution functions*, Z. Physik
763 B Cond. Mat. **43**(2), 119 (1981), doi:10.1007/BF01293604.
- 764 [83] A. D. Bruce and N. B. Wilding, *Scaling fields and universality of the liquid-gas critical*
765 *point*, Phys. Rev. Lett. **68**, 193 (1992), doi:10.1103/PhysRevLett.68.193.
- 766 [84] V. Aji and N. Goldenfeld, *Fluctuations in finite critical and turbulent systems*, Phys. Rev.
767 Lett. **86**, 1007 (2001), doi:10.1103/PhysRevLett.86.1007.
- 768 [85] S. T. Bramwell, P. C. W. Holdsworth and J.-F. Pinton, *Universality of rare fluctuations in*
769 *turbulence and critical phenomena*, Nature **396**, 552 (1998), doi:10.1038/25083.
- 770 [86] V. Eisler, Z. Rácz and F. van Wijland, *Magnetization distribution in the transverse Ising*
771 *chain with energy flux*, Phys. Rev. E **67**, 056129 (2003), doi:10.1103/PhysRevE.67.056129.
- 772 [87] R. W. Cherng and E. Demler, *Quantum noise analysis of spin systems realized with cold*
773 *atoms*, New Journal of Physics **9**(1), 7 (2007), doi:10.1088/1367-2630/9/1/007.

- 774 [88] S. Groha, F. H. L. Essler and P. Calabrese, *Full counting statistics in the transverse field*
775 *Ising chain*, SciPost Phys. **4**, 43 (2018), doi:10.21468/SciPostPhys.4.6.043.
- 776 [89] N. Wu, *Exact one- and two-site reduced dynamics in a finite-size quantum Ising ring after a*
777 *quench: a semi-analytical approach* (2021), 2103.12509.
- 778 [90] K. Najafi, M. A. Rajabpour and J. Viti, *Return amplitude after a quantum quench in the XY*
779 *chain*, Journal of Statistical Mechanics: Theory and Experiment **2019**(8), 083102 (2019),
780 doi:10.1088/1742-5468/ab3413.
- 781 [91] F. Ares, M. A. Rajabpour and J. Viti, *Exact full counting statistics for the staggered magne-*
782 *tization and the domain walls in the XY spin chain* (2020), 2012.14012.
- 783 [92] M. Białończyk and B. Damski, *Dynamics of longitudinal magnetization in transverse-field*
784 *quantum Ising model: from symmetry-breaking gap to Kibble-Zurek mechanism*, Journal of
785 Statistical Mechanics: Theory and Experiment **2020**(1), 013108 (2020), doi:10.1088/1742-
786 5468/ab609a.
- 787 [93] N. Wu, *Longitudinal magnetization dynamics in the quantum Ising ring: A Pfaffian method*
788 *based on correspondence between momentum space and real space*, Phys. Rev. E **101**,
789 042108 (2020), doi:10.1103/PhysRevE.101.042108.
- 790 [94] S.-J. GU, *Fidelity approach to quantum phase transitions*, International Journal of Modern
791 Physics B **24**(23), 4371 (2010), doi:10.1142/S0217979210056335.